Spontaneous emission and absorption properties of a driven three-level system

L. M. Narducci* and M. O. Scully
Center for Advanced Studies, University of New Mexico, Albuquerque, New Mexico 87131

G.-L. Oppo
Department of Physics and Applied Physics, University of Strathclyde, Glasgow, G4 0NG Scotland, United Kingdom

P. Ru and J. R. Tredicce
Department of Physics and Atmospheric Science, Drexel University, Philadelphia, Pennsylvania 19104
(Received 2 April 1990)

We investigate the steady-state spontaneous emission spectrum of a three-level atom driven by two coherent fields and the absorption spectrum of a weak probe passing through a collection of such driven atoms. We find that the fluorescence spectrum is strongly affected by the decay rates of all the levels involved in the atomic evolution and not just by the decay parameters of the specific transition whose emission spectrum is being monitored. In particular, the spectral components can acquire very different widths and peak heights relative to the case of the standard resonance fluorescence in which a two-level system is driven by a single near-resonant field. An external probe signal passing through the gas of three-level atoms may be absorbed or amplified, as in the standard two-level case, but under specific operating conditions, amplification (or absorption) occurs over the entire range where the atomic response is appreciable. In this case the existence of amplification or absorption is controlled solely by the population difference between two dressed states of the system. We provide numerical results in support of our arguments for arbitrary values of the atomic and field parameters and also develop an analytic description in the limit of strong driving fields that leads to explicit line-shape and linewidth formulas.

I. INTRODUCTION

Spontaneous emission is probably one of the best known fundamental processes resulting from the interaction between radiation and matter. When an excited atom decays into a vacuum, the emitted radiation has an isotropic distribution in space and its spectrum is a Lorentzian function of frequency with a bandwidth proportional to the Einstein spontaneous decay rate.[1,2] We have known for quite some time that the spectrum of spontaneous emission can be altered in a fundamental way by driving the atom with a sufficiently strong resonant field. In fact, according to the theory,[3–6] and as confirmed by many accurate experiments,[7–10] the incoherent part of the spectrum produced by a resonantly driven atom develops sidebands which are about $\frac{1}{3}$ as high as the central peak, are removed from the resonance by an amount proportional to the Rabi frequency of the driving field, and are wider than the central peak by a factor 1.5. In addition, the linewidths of both the central peak and the sidebands are governed by the Einstein spontaneous decay rate in the absence of collision effects.

The growth of experimental sophistication has revealed new and more exotic behaviors, such as one observes when excited atoms decay within the enclosure of an electromagnetic resonator.[11] Experiments have shown that it is possible to alter the density of electromagnetic modes in the neighborhood of the resonant frequency and to control the rate of spontaneous emission from an excited atom; this rate can be enhanced if one of the resonances of a high-Q cavity coincides with the chosen atomic transition, or reduced if the resonator cutoff wavelength is smaller than the wavelength of the spontaneously emitted photons. The change in decay lifetime can be understood fairly readily by considering the accessible modes into which excited atoms can radiate. If the modal density in the vicinity of the frequency of interest is less than that of empty space the atom's decay will be retarded, if it is greater it will be accelerated.

Apparently, it is not necessary to tamper with the density of decay channels or to employ sophisticated resonators if one wishes to modify the spontaneous emission spectrum of an excited atom. In fact, as we propose in this paper, it may be possible to observe spontaneous emission in empty space with a linewidth which is significantly different from the natural linewidth, where by "natural" we mean the linewidth "calculated within the framework of the standard Wigner-Weisskopf theory." With appropriate selection of atomic and experimental parameters, the linewidth of a given spontaneous transition may be varied almost continuously and, in particular, it may be made even narrower than the natural linewidth.

In this paper we reconsider the response of a three-level atom driven by two optical fields with the aim of calculating the spontaneous emission spectrum and the absorption spectrum of a weak tunable probe. This general setting has already been the focus of many investiga-

tions on optical pumping, double resonance, and nonlinear spectroscopy, for example,[12] in addition to both experimental and theoretical contributions of immediate relevance to this work.[13–19] Here we stress that the addition of a second driving field to the traditional arrangement of resonance fluorescence not only causes qualitative changes in the shape of the emission and absorption[20] spectra but it also modifies the linewidth in a way that depends on the atomic parameters and the relative strength of the fields.[21] Of course the atomic parameters allow only a limited selection of operating conditions in practical situations, but the driving field strengths should be controllable over a sufficiently wide range to allow a verification of most of our predictions.

The system of interest to this work is illustrated schematically in Fig. 1. The arrows denote the two driving fields with carrier frequencies ω_1 and ω_2, respectively, which may be detuned from the exact resonances by the offsets Δ_1 and Δ_2. The atomic transitions $1\rightarrow 3$ and $1\rightarrow 2$ are assumed to be optically allowed, while the transition $2\rightarrow 3$ is forbidden on the basis of parity considerations. The downward decay rates between levels i and j are denoted with W_{ij}. This arrangement is usually known as a V system. Two alternative configurations, the Λ and the cascade (or Ξ) systems, are illustrated in Figs. 2(a) and 2(b). Here we focus almost exclusively on the radiative and absorbing properties of the V system because it appears to be the most favorable to emphasize line narrowing features which we believe are the most interesting and novel aspect of this work. A detailed comparison with the Λ and Ξ models will be presented elsewhere.

The main result of this work is the derivation of exact formulas for the emission spectra of the $3\rightarrow 1$ and $2\rightarrow 1$ transitions and for the absorption spectra of a tunable weak probe in the neighborhood of these transitions. Our results are valid for arbitrary strengths of the driving fields and generalize the well-known resonance fluorescence spectra of a two-level system. For example, the $3\rightarrow 1$ emission spectrum reacquires the standard form predicted in Refs. 3–6 when field 2 is turned off and the decay rate W_{32} is set equal to zero. They also complement and extend earlier studies by Cohen-Tannoudji and Reynaud [see especially Ref. 15(c)] which were directed mainly to the case of sufficiently large driving field strengths.

One drawback of this calculation is that the formulas describing the emission and absorption spectra cannot be cast into a transparent and readily interpretable form.

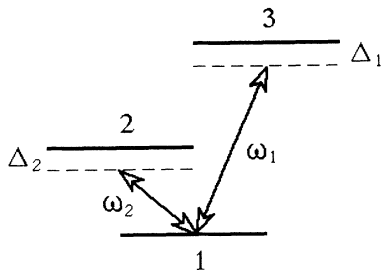

FIG. 1. Schematic representation of the V model; ω_1 and ω_2 are the carrier frequencies of the driving fields and Δ_1 and Δ_2 the respective detuning parameters.

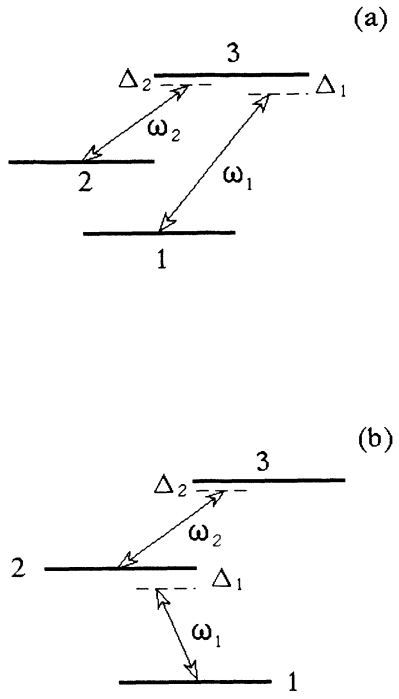

FIG. 2. (a) Schematic representation of the Λ model; (b) schematic representation of the cascade or Ξ model. The meaning of the symbols is the same as in Fig. 1.

However, they are ideally suited for simple numerical calculations, as we illustrate in Sec. IV. They also allow the derivation of a simple procedure by which the high-intensity limit can be extracted with little effort and very good accuracy. Our limiting expressions for the emission spectra agree, for the most part, with the results of Ref. 15(c) (properly applied to the case of a V system). We also predict the appearance of five spectral components in resonance, one centered at the atomic transition frequency and two symmetric pairs of sidebands spaced by $\pm G$ and $\pm 2G$ from the center, where $G=(g_1^2+g_2^2)^{1/2}$ can be called the effective Rabi frequency, and g_1 and g_2 are the individual Rabi frequencies of the driving fields. The central peak and the $\pm 2G$ sidebands have a Lorentzian profile whose width and peak heights agree with those quoted in Ref. 15(c). The $\pm G$ sidebands, however, do not have a Lorentzian shape and have a different linewidth, the origin of which can be traced, perhaps, to the different handling of the irreversible decay processes in the two approaches. However, the actual origin of this small discrepancy is not yet completely clear.

An important conclusion of the asymptotic calculation, and one that is exhibited particularly well by the V model, is that under appropriate conditions the linewidth of the spontaneous emission spectrum of the driven atom can become considerably narrower than the value predicted by the Wigner-Weisskopf theory. This point will be properly emphasized in the main text.

An additional useful spin-off is the derivation of explicit formulas for the absorption spectra in the high-intensity limit. Here the dressed state approach, that was already shown to be so useful in Ref. 15, pays off most convincingly. In this limit, in fact, we discover that, sub-

ject to a condition requiring population inversion between two dressed states, the absorption spectrum becomes a gain spectrum over the entire frequency range where the atomic response is appreciable. Of course the appearance of a frequency domain where an external probe is amplified instead of being absorbed is not new. The novelty here is that the entire profile turns into a gain profile, if the above inversion condition is satisfied. Superficially this result is reminiscent of the so-called "laser without inversion"[22] but, as we indicate in Sec. V, the existence of a gain profile in our case is accompanied by the simultaneous population inversion of levels 2-1 and 3-1.

This paper is organized as follows. In Sec. II we assemble the theoretical tools for the calculation of the emission and absorption spectra from the driven atom, and in Sec. III we derive the specific expressions related to these observable quantities. Section IV is dedicated to a survey of the most significant spectral results. A deeper look into the mechanism that is responsible for the linewidth variation is provided in Sec. V; here we solve the master equation for the driven atom in the limit of a strong effective Rabi frequency with the help of appropriate dressed atomic states,[15,19] and we derive analytic expressions for the main spectral structures, their linewidths, and peak heights. Section VI contains a summary, an overview of our results, and a discussion of future developments.

II. DESCRIPTION OF THE MODEL AND EQUATIONS OF MOTION

We are interested in the evolution of a three-level system (Fig. 1) driven by two external fields whose carrier frequencies ω_1 and ω_2 are resonant or nearly resonant with the atomic transitions $1\rightarrow 3$ and $1\rightarrow 2$, respectively. Our aim is to calculate the spectrum of the radiation emitted spontaneously by the atom and the frequency dependence of the absorption coefficient of a weak probe (absorption spectrum).

Following the procedure adopted in Ref. 23, our program evolves along the following lines. First, we derive the master equation for the three-level system in the semiclassical approximation, i.e., under the assumption that both driving fields can be described by c-number functions. Next, we take advantage of the fact that the scattered electromagnetic field in the far zone is proportional to the atomic polarization operator to calculate the field correlation function and the spectrum of the emitted radiation. The absorption spectrum of a weak probe, according to the standard linear-response theory is proportional to the unequal time commutator of field operators.[24] For the same reason mentioned before, also this quantity can be expressed and calculated in terms of atomic operators. The emission and absorption spectra require knowledge of expectation values of products of operators calculated at different times; we handle these quantities with the help of the quantum regression theorem.[25]

The Hamiltonian of the three-level system interacting with two classical fields is given by

$$H=\sum_{i=1}^{3}\varepsilon_i a_i^\dagger a_i+\hbar g_1(e^{-i\omega_1 t}a_3^\dagger a_1+e^{i\omega_1 t}a_1^\dagger a_3)+\hbar g_2(e^{-i\omega_2 t}a_2^\dagger a_1+e^{i\omega_2 t}a_1^\dagger a_2)\ , \tag{2.1}$$

where ε_i $(i=1,2,3)$ are the energies of the three stationary states of the atom, g_1 and g_2 are the Rabi frequencies of the driving fields, and $a_i^\dagger, a_i$ $(i=1,2,3)$ are fermion operators that describe the creation of an electron in level i or its removal.

Consider first the reversible part of the Liouville equation in the interaction representation. This has the form

$$\frac{\partial\rho'}{\partial t}=-\frac{i}{\hbar}[H_1',\rho']\ , \tag{2.2}$$

where

$$H_1'=\hbar g_1(a_3^\dagger a_1 e^{i\Delta_1 t}+a_1^\dagger a_3 e^{-i\Delta_1 t})+\hbar g_2(a_2^\dagger a_1 e^{i\Delta_2 t}+a_1^\dagger a_2 e^{-i\Delta_2 t}) \tag{2.3}$$

and

$$\Delta_1=\omega_{31}-\omega_1\ , \tag{2.4a}$$

$$\Delta_2=\omega_{21}-\omega_2\ . \tag{2.4b}$$

The prime denotes the interaction representation and ω_{31} and ω_{21} are atomic transition frequencies. The matrix elements of ρ' according to Eq. (2.2) satisfy linear coupled equations of motion containing explicit time-dependent factors of the complex exponential type. These can be removed with the transformation

$$\begin{aligned} R_{ii}&=\rho_{ii}' \quad (i=1,2,3)\ ,\\ R_{12}&=\rho_{12}' e^{i\Delta_2 t}\ ,\\ R_{13}&=\rho_{13}' e^{i\Delta_1 t}\ ,\\ R_{23}&=\rho_{23}' e^{i(\Delta_1-\Delta_2)t}\ , \end{aligned} \tag{2.5}$$

whose effect is to produce autonomous equations for the matrix elements R_{ij}; we would like to stress that the absence of explicit time dependence in the equations of motion plays an important role for the implementation of our procedure. Next we consider the irreversible part of the atomic dynamics. This is described by the master equation for the arbitrary multilevel system[26]

$$\left[\frac{\partial\rho'}{\partial t}\right]_{\text{irrev}}\equiv\Lambda\rho'=\sum_{i,j}[a_i^\dagger a_j\rho' a_j^\dagger a_i(A_{jiij}+A_{jiij}^*)-a_j^\dagger a_j\rho' A_{jiij}-\rho' a_j^\dagger a_j A_{jiij}^*]\ , \tag{2.6}$$

where A_{jiij} are complex rate constants related to the population transition rates W_{ij}, the polarization decay rates γ_{ij}, and the frequency shifts $\Delta\Omega_{ij}$ by

$$W_{ij}=A_{jiij}+A_{jiij}^*\ , \tag{2.7a}$$

$$\gamma_{ij}=\sum_k \mathrm{Re}(A_{ikki}+A_{jkkj}^*)=\tfrac{1}{2}\sum_k(W_{ik}+W_{jk})\ , \tag{2.7b}$$

$$\Delta\Omega_{ij}=-\sum_k \mathrm{Im}(A_{jkkj}+A_{ikki}^*)\ . \tag{2.7c}$$

In the following we shall ignore both level shifts and pure phase relaxation effects due to elastic collisions (i.e., we assume $A_{iiii}=0$). Note, in addition, that

$$\mathrm{Re}\,A_{ijji}=\mathrm{Re}\,A_{jiij}\exp\left[\frac{\hbar\omega_{ij}}{kT}\right], \tag{2.8}$$

where ω_{ij} is the transition frequency between levels i and j and T is the absolute temperature. From Eq. (2.8) it follows that the rates of excitation from a lower to a higher level due to collisional effects can be safely ignored as long as the energy separation between the levels is much larger than kT. Because one may encounter situations where this condition is not fulfilled, for completeness we continue to include the rate coefficients W_{ij} with $i<j$, although in our numerical simulations we shall set them equal to zero.

The full master equation is

$$\frac{\partial\rho'}{\partial t}=-\frac{i}{\hbar}[H_1',\rho']+\Lambda\rho' . \tag{2.9}$$

In terms of the variables R_{ij} Eq. (2.9) takes the explicit form

$$\begin{aligned}
\frac{dR_{12}}{d\tau}&=i\tilde{\Delta}_2R_{12}-i\beta_1R_{32}-i\beta_2(R_{22}-R_{11})-\tilde{\gamma}_{12}R_{12} ,\\
\frac{dR_{13}}{d\tau}&=i\tilde{\Delta}_1R_{13}-i\beta_1(R_{33}-R_{11})-i\beta_2R_{23}-\tilde{\gamma}_{13}R_{13} ,\\
\frac{dR_{22}}{d\tau}&=-i\beta_2(R_{12}-R_{21})+\tilde{W}_{12}R_{11}+\tilde{W}_{32}R_{33}\\
&\quad-(\tilde{W}_{21}+\tilde{W}_{23})R_{22} ,\\
\frac{dR_{23}}{d\tau}&=i(\tilde{\Delta}_1-\tilde{\Delta}_2)R_{23}+i\beta_1R_{21}-i\beta_2R_{13}-\tilde{\gamma}_{23}R_{23} ,\\
\frac{dR_{33}}{d\tau}&=-i\beta_1(R_{13}-R_{31})+\tilde{W}_{13}R_{11}+\tilde{W}_{23}R_{22}\\
&\quad-(1+\tilde{W}_{32})R_{33} ,
\end{aligned} \tag{2.10}$$

where

$$\begin{aligned}
&R_{11}=1-R_{22}-R_{33},\quad R_{21}=R_{12}^*,\quad R_{31}=R_{13}^* ,\\
&R_{32}=R_{23}^* .
\end{aligned} \tag{2.11}$$

In arriving at Eqs. (2.10) we have introduced the dimensionless time $\tau=W_{31}t$ and the scaled Rabi frequencies $\beta_1=g_1/W_{31}$, and $\beta_2=g_2/W_{31}$. The remaining rate constants are scaled to W_{31} and labeled with a tilde.

For the purpose of the following development it is convenient to represent the set of eight linearly independent equations for the matrix elements R_{ij} in the compact form

$$\frac{d}{d\tau}\psi=L\psi+\mathbf{I} , \tag{2.12}$$

where the eight components of the vector ψ are defined by

$$\begin{aligned}
&\psi_1=R_{12},\quad \psi_2=R_{31},\quad \psi_3=R_{21},\quad \psi_4=R_{22} ,\\
&\psi_5=R_{23},\quad \psi_6=R_{31},\quad \psi_7=R_{32},\quad \psi_8=R_{33} ,
\end{aligned} \tag{2.13}$$

and L is the (8×8) matrix

$$L=\begin{pmatrix}
-(\tilde{\gamma}_{12}-i\tilde{\Delta}_2) & 0 & 0 & -2i\beta_2 & 0 & 0 & -i\beta_1 & -i\beta_2\\
0 & -(\tilde{\gamma}_{13}-i\tilde{\Delta}_1) & 0 & -i\beta_1 & 0 & 0 & 0 & -2i\beta_1\\
0 & 0 & -(\tilde{\gamma}_{12}+i\tilde{\Delta}_2) & 2i\beta_2 & i\beta_1 & 0 & 0 & i\beta_2\\
-i\beta_2 & 0 & i\beta_2 & -(\tilde{W}_{12}+\tilde{W}_{21}+\tilde{W}_{23}) & 0 & 0 & 0 & -(\tilde{W}_{12}-\tilde{W}_{32})\\
0 & -i\beta_2 & i\beta_1 & 0 & -[\tilde{\gamma}_{23}-i(\tilde{\Delta}_1-\tilde{\Delta}_2)] & 0 & 0 & 0\\
0 & 0 & 0 & i\beta_1 & 0 & -(\tilde{\gamma}_{13}+i\tilde{\Delta}_1) & i\beta_2 & 2i\beta_1\\
-i\beta_1 & 0 & 0 & 0 & 0 & i\beta_2 & -[\tilde{\gamma}_{23}+i(\tilde{\Delta}_1-\tilde{\Delta}_2)] & 0\\
0 & -i\beta_1 & 0 & (\tilde{W}_{23}-\tilde{W}_{13}) & 0 & i\beta_1 & 0 & -(1+\tilde{W}_{12}+\tilde{W}_{13})
\end{pmatrix} \tag{2.14}$$

The vector **I** is an inhomogeneous term with components

$$I_1=i\beta_2,\quad I_2=i\beta_1,\quad I_3=-i\beta_2,\quad I_4=\tilde{W}_{12}\ ,$$
$$I_5=0,\quad I_6=-i\beta_1,\quad I_7=0,\quad I_8=\tilde{W}_{13}\ . \tag{2.15}$$

Because, as already mentioned, our calculation of the quantities of interest involves the quantum regression theorem, we will need explicit expressions for the variables ψ_i $(i=1,2,\ldots,8)$ in terms of their initial values. This is done conveniently in Laplace space. Thus, if τ_0 denotes an arbitrary initial time, the Laplace transform of Eq. (2.12) yields

$$\hat{\boldsymbol{\psi}}(z)=M(z)\boldsymbol{\psi}(\tau_0)+\frac{1}{z}M(z)\mathbf{I} \tag{2.16}$$

or in component form

$$\hat{\psi}_i(z)=\sum_j M_{ij}(z)\psi_j(\tau_0)+\frac{1}{z}\sum_j M_{ij}(z)I_j\ , \tag{2.17}$$

where

$$M=(z-L)^{-1}\ . \tag{2.18}$$

Note that in steady state [see Eq. (2.12)] we have

$$\boldsymbol{\psi}(\infty)=-L^{-1}\mathbf{I} \tag{2.19}$$

or, explicitly, in component form

$$\psi_i(\infty)=-\sum_j (L^{-1})_{ij}I_j\ . \tag{2.20}$$

III. CALCULATION OF THE SPECTRA

In this section we derive the steady-state spectrum of resonance fluorescence and the absorption spectrum of a weak probe. This calculation is made possible by the link between the scattered field and the atomic polarization operator which in the far zone takes the form

$$\mathbf{E}^{(+)}(\mathbf{r},t)=\mathbf{E}_0^{(+)}(\mathbf{r},t)-\frac{\omega_0^2}{c^2 r}\hat{\mathbf{n}}\times(\hat{\mathbf{n}}\times\hat{\mathbf{d}})P^{(+)}\left[t-\frac{r}{c}\right]\ , \tag{3.1}$$

where $\mathbf{E}^{(+)}$ is the positive part of the total field operator, $\mathbf{E}_0^{(+)}$ is the corresponding solution of the homogeneous wave equation, and $\hat{\mathbf{n}}$ and $\hat{\mathbf{d}}$ are unit vectors in the direction of observation and along the atomic dipole moment, respectively. Away from the forward direction, the field and the atomic polarization operators are directly proportional to each other. Hence, we only need to limit our considerations to the atomic correlation function

$$\Gamma^{(1)}(\tau_1,\tau_0)=\langle P^{(-)}(\tau_1)P^{(+)}(\tau_0)\rangle\ . \tag{3.2}$$

The Fourier transform of Eq. (3.2) is proportional to the emission spectrum and, as explained below, is also linked to the absorption spectrum of a weak probe.

A. The spectrum of resonance fluorescence

The total polarization operator of the three-level atom is given by

$$P(\tau)=\mu_{12}(a_1^\dagger a_2+a_2^\dagger a_1)+\mu_{13}(a_1^\dagger a_3+a_3^\dagger a_1)\ , \tag{3.3}$$

where μ_{ij} are the moduli of the induced transition dipole moments and where we have assumed $\mu_{23}=0$. The positive and negative parts of the polarization operator are given by

$$P^{(+)}(t)=\mu_{12}a_1^\dagger a_2+\mu_{13}a_1^\dagger a_3\ , \tag{3.4a}$$

$$P^{(-)}(t)=[P^{(+)}(t)]^\dagger\ . \tag{3.4b}$$

Our calculation of Eq. (3.2a) involves a straightfoward but laborious application of the quantum regression theorem. This theorem[25(c)] states that if M, Q, and N are members of a complete set of system operators $\{S_\mu\}$ and if the one-time averages can be expressed in the form

$$\langle M(\tau)\rangle=\sum_\mu O_\mu(\tau,\tau')\langle S_\mu(\tau')\rangle,\quad \tau'<\tau \tag{3.5}$$

where $O_\mu(\tau,\tau')$ are c-number functions of time, then two-time expectation values take the form

$$\langle Q(\tau')M(\tau)N(\tau')\rangle=\sum_\mu O_\mu(\tau,\tau')\langle Q(\tau')S_\mu(\tau')N(\tau')\rangle,\quad \tau'<\tau\ . \tag{3.6}$$

In particular, Q or N can be identified with the identity operator. In the remainder of this subsection we outline the main steps of this calculation.

The starting point is the one-time average

$$\langle P^{(-)}(\tau_1)\rangle=\mathrm{Tr}[\rho(\tau_1)(\mu_{12}a_2^\dagger a_1+\mu_{13}a_3^\dagger a_1)]\ , \tag{3.7}$$

which can be written in terms of $\psi_1(\tau_1),\psi_2(\tau_1)$ as follows:

$$\langle P^{(-)}(\tau_1)\rangle=\mu_{12}e^{i\omega_2\tau_1}\psi_1(\tau_1)+\mu_{13}e^{i\omega_1\tau_1}\psi_2(\tau_1)\ . \tag{3.8}$$

At this point the essential step is to express each of the matrix elements $\psi_i(\tau_1)$ that appear in Eq. (3.8) in terms of their "initial" values at $\tau=\tau_0$. While this could be done beginning with the formal integration of Eq. (2.12), here we operate in the space of the Laplace transform. Thus, Eq. (3.8) yields

$$\langle\hat{P}^{(-)}(z)\rangle=\mu_{12}\hat{\psi}_1(z_2)+\mu_{13}\hat{\psi}_2(z_1)\ , \tag{3.9}$$

where

$$z_1=z-i\omega_1,\quad z_2=z-i\omega_2\ . \tag{3.10}$$

With the help of Eq. (2.17), Eq. (3.9) can be cast into the required form

$$\langle\hat{P}^{(-)}(z)\rangle=\sum_j[\mu_{12}M_{1j}(z_2)+\mu_{13}M_{2j}(z_1)]\psi_j(\tau_0)+\sum_j\left[\frac{\mu_{12}}{z_2}M_{1j}(z_2)+\frac{\mu_{13}}{z_1}M_{2j}(z_1)\right]I_j\ . \tag{3.11}$$

Next we must express $\psi_j(\tau_0)$ and I_j in the form of expectation values of system operators at $\tau=\tau_0$. This can be done directly from the definition of $\psi_j(\tau_0)$ as illustrated by the following example:

$$\psi_1(\tau_0)=e^{-i\omega_2\tau_0}\rho_{12}(\tau_0)=e^{-i\omega_2\tau_0}\langle|2\rangle\langle1|\rangle_{\tau_0}\ . \tag{3.12}$$

In addition, the inhomogeneous term I_j can also be written as

$$I_j = I_j \mathrm{Tr}[\rho(\tau_0)] = I_j \langle \mathbb{1} \rangle_{\tau_0} , \tag{3.13}$$

where $\mathbb{1}$ is the identity operator. According to the regression theorem, the correlation function $\langle \hat{P}^{(-)}(z) P^{(+)}(\tau_0) \rangle$ can be obtained from the above expression for $\langle \hat{P}^{(-)}(z) \rangle$ by replacing every expectation value of the type $\langle |i\rangle\langle j| \rangle_{\tau_0}$ with $\langle |i\rangle\langle j| P^{(+)}(\tau_0) \rangle_{\tau_0}$. Consider, for example, the expectation value $\langle |2\rangle\langle 1| \rangle_{\tau_0}$; in this case we have

$$\begin{aligned} \langle |2\rangle\langle 1| \rangle_{\tau_0} &\to \langle |2\rangle\langle 1| P^{(+)}(\tau_0) \rangle_{\tau_0} \\ &= \mu_{12} \rho_{22}(\tau_0) + \mu_{13} \rho_{32}(\tau_0) \\ &= \mu_{12} \psi_4(\tau_0) + \mu_{13} e^{-i(\omega_1 - \omega_2)\tau_0} \psi_7(\tau_0) . \end{aligned} \tag{3.14}$$

In a similar way we have

$$\begin{aligned} \langle \mathbb{1} \rangle_{\tau_0} &\to \langle P^{(+)}(\tau_0) \rangle \\ &= \mu_{12} e^{-i\omega_2 \tau_0} \psi_3(\tau_0) + \mu_{13} e^{-i\omega_1 \tau_0} \psi_6(\tau_0) . \end{aligned} \tag{3.15}$$

The polarization correlation function contains three types of oscillating exponentials,

$$\exp(i\Omega\tau_0), \quad \exp(i\Omega\tau_1), \quad \exp[i\Omega(\tau_1 - \tau_0)] , \tag{3.16}$$

where Ω is an optical frequency. Because we are interested in the steady-state emission spectrum we take the double limit

$$\tau_0, \tau_1 \to \infty \tag{3.17}$$

with $\tau_1 - \tau_0$ being finite. The only surviving terms are those whose oscillating exponentials involve the time difference $\tau_1 - \tau_0$. A detailed analysis of the full correlation function leads to the following result:

$$\begin{aligned} \langle \hat{P}^{(-)}(z) P^{(+)}(\infty) \rangle = \mu_{12}^2 & \left[M_{11}(z_2) \psi_4(\infty) + M_{12}(z_2) \psi_5(\infty) + \sum_j \frac{1}{z_2} M_{1j}(z_2) I_j \psi_3(\infty) \right] \\ + \mu_{13}^2 & \left[M_{21}(z_1) \psi_7(\infty) + M_{22}(z_1) \psi_8(\infty) + \sum_j \frac{1}{z_1} M_{2j}(z_1) I_j \psi_6(\infty) \right] . \end{aligned} \tag{3.18}$$

Equation (3.18) shows that the spectrum of resonance fluorescence is composed of two separate structures with center frequencies located at ω_2 and ω_1, respectively, and magnitudes proportional to the dipole moments of the two atomic transitions. Each contribution to the total spectrum has the generic form

$$f(z) = \frac{A}{z} + g(z) , \tag{3.19}$$

where A is a constant and $g(z)$ is an analytic function of z for $\mathrm{Re}z \geq 0$. The singularity reflects the existence of a coherent Rayleigh peak whose origin can be traced to the elastic scattering of the driving fields, while $g(z)$ describes the incoherent part of the spectrum of the emitted radiation. If we denote the full correlation function with

$$\hat{\Gamma}^{(1)}(z) \equiv \langle \hat{P}^{(-)}(z) P^{(+)}(\infty) \rangle , \tag{3.20}$$

the incoherent part can be calculated according to the simple algorithm

$$\begin{aligned} \hat{\Gamma}^{(1)}_{\mathrm{incoh}}(z) = \hat{\Gamma}^{(1)}(z) & - \frac{1}{z_1} \lim_{z_1 \to 0} z_1 \hat{\Gamma}^{(1)}(z) \\ & - \frac{1}{z_2} \lim_{z_2 \to 0} z_2 \hat{\Gamma}^{(1)}(z) . \end{aligned} \tag{3.21}$$

Finally, the required emission spectrum is given by

$$S(\omega) = \mathrm{Re} \hat{\Gamma}^{(1)}_{\mathrm{incoh}}(z)|_{z = i\omega} , \tag{3.22}$$

where

$$\begin{aligned} \hat{\Gamma}^{(1)}_{\mathrm{incoh}}(z) = \mu_{12}^2 & \left[M_{11}(z_2) \psi_4(\infty) + M_{12}(z_2) \psi_5(\infty) + \sum_j N_{1j}(z_2) I_j \psi_3(\infty) \right] \\ + \mu_{13}^2 & \left[M_{21}(z_1) \psi_7(\infty) + M_{22}(z_1) \psi_8(\infty) + \sum_j N_{2j}(z_1) I_j \psi_6(\infty) \right] \end{aligned} \tag{3.23}$$

and

$$N_{ij}(z) = (L^{-1}(z - L)^{-1})_{ij} . \tag{3.24}$$

The results of Eqs. (3.22) and (3.23) can be converted into numerical form by standard matrix manipulation techniques. They suffer, however, from a drawback because the complicated structure of the matrix elements $M_{ij}(z)$ and $N_{ij}(z)$ makes them uninterpretable in simple physical grounds. This problem will be overcome in part in Sec. V where we show how to obtain a simpler expression for the spectra in the limit of large effective Rabi frequency. Typical predictions based on the numerical evaluation of Eq. (3.23) will be shown in Sec. IV.

B. The absorption spectrum of a weak probe

We now turn our attention to a related problem: the three-level system is driven by the external fields at fre-

quencies ω_1 and ω_2 and is probed by a tunable weak beam whose attenuation (or amplification) is measured in transmission. According to the linear-response theory[24] the exponential attenuation coefficient at a given frequency ω is given by

$$A(\omega)=\text{const}\times\mathcal{F}\{\langle[P^{(-)}(\tau_1),P^{(+)}(\tau_0)]\rangle\}\ , \tag{3.25}$$

where $\mathcal{F}$ denotes the Fourier transform operator. The square brackets indicate the unequal time commutator and the quantum ensemble average $\langle\ \rangle$ must be carried out under steady-state conditions, i.e., in the limit (3.17).

The absorption spectrum is composed of two parts: the first, $\langle P^{(-)}(\tau_1)P^{(+)}(\tau_0)\rangle$, is identical to the one calculated in Sec. III A; the second, $\langle P^{(+)}(\tau_0)P^{(-)}(\tau_1)\rangle$, can be derived following the same procedure with minor modifications. The starting point in Laplace space is the single-time average

$$\langle\hat{P}^{(-)}(z)\rangle=\mu_{12}\hat{\psi}_1(z_2)+\mu_{13}\hat{\psi}_2(z_1) \tag{3.26}$$

whose explicit form is

$$\langle\hat{P}^{(-)}(z)\rangle=\sum_j\mu_{12}M_{1j}(z_2)+\mu_{13}M_{2j}(z_1)]\psi_j(\tau_0)+\sum_j\left[\frac{\mu_{12}}{z_2}M_{1j}(z_2)+\frac{\mu_{13}}{z_1}M_{2j}(z_1)\right]I_j\ . \tag{3.27}$$

Again, we must express $\psi_j(\tau_0)$ and I_j in terms of expectation values of system operators and then replace every expectation value of the type $\langle|i\rangle\langle j|\rangle_{\tau_0}$ and $\langle\mathbf{1}\rangle_{\tau_0}$ with $\langle P^{(+)}(\tau_0)|i\rangle\langle j|\rangle_{\tau_0}$ and $\langle P^{(+)}(t_0)\rangle_{\tau_0}$, respectively, where $P^{(+)}(\tau_0)$ is given by Eq. (3.4b). Thus, for example, we have

$$\psi_1(\tau_0)=e^{-i\omega_2\tau_0}\langle|2\rangle\langle1|\rangle_{\tau_0}\rightarrow e^{-i\omega_2\tau_0}\mu_{12}[1-\psi_4(\tau_0)-\psi_8(\tau_0)] \tag{3.28}$$

and

$$I_j=I_j\text{Tr}[\rho(\tau_0)]\rightarrow I_j[\mu_{12}e^{-i\omega_2\tau_0}\psi_3(\tau_0)+\mu_{13}e^{-i\omega_1\tau_0}\psi_6(\tau_0)]\ . \tag{3.29}$$

Similar expressions hold for the remaining expectation values. At this point, as in the case of the emission spectrum, we must sort out the terms that survive the steady-state limit with the result

$$\langle P^{(+)}(\infty)\hat{P}^{(-)}(z)\rangle=\mu_{12}^2\left[M_{11}(z_2)[1-\psi_4(\infty)-\psi_8(\infty)]+M_{14}(z_2)\psi_3(\infty)+M_{17}(z_2)\psi_6(\infty)+\sum_j\frac{1}{z_2}M_{1j}(z_2)I_j\psi_3(\infty)\right]+\mu_{13}^2\left[M_{22}(z_1)[1-\psi_4(\infty)-\psi_8(\infty)]+M_{25}(z_1)\psi_3(\infty)+M_{28}(z_1)\psi_6(\infty)+\sum_j\frac{1}{z_1}M_{2j}(z_1)I_j\psi_6(\infty)\right]\ . \tag{3.30}$$

Finally, the complete expression of the absorption spectrum (in Laplace space) is given by

$$\begin{aligned}\langle[\hat{P}^{(-)}(z),P^{(+)}(\tau_0)]\rangle&=\langle\hat{P}^{(-)}(z)P^{(+)}(\tau_0)\rangle-\langle P^{(+)}(\tau_0)\hat{P}^{(-)}(\tau_0)\rangle\\&=\mu_{12}^2[M_{11}(z_2)\psi_4+M_{12}(z_2)\psi_5-M_{11}(z_2)(1-\psi_4-\psi_8)-M_{14}(z_2)\psi_3-M_{17}(z_2)\psi_6]\\&\quad+\mu_{13}^2[M_{21}(z_1)\psi_7+M_{22}(z_1)\psi_8-M_{22}(z_1)(1-\psi_4-\psi_8)-M_{25}(z_1)\psi_3-M_{28}(z_1)\psi_6]\end{aligned} \tag{3.31}$$

and

$$A(\omega)=\text{Re}\langle[\hat{P}^{(-)}(z),P^{(+)}(\tau_0)]\rangle_{z=i\omega}\ . \tag{3.32}$$

The absorption spectrum, just as the spectrum of resonance fluorescence, is composed of two separate structures centered around the transition frequencies of the atom. The numerical analysis of the results of this subsection is also assembled in Sec. IV.

IV. DISCUSSION OF THE EMISSION AND ABSORPTION SPECTRA

This section contains a graphical survey of some specific predictions that emerge from the formulas derived in Sec. III. In our numerical work the time is measured in units of W_{31}^{-1} (i.e., $\tau=W_{31}t$), the scaled Rabi frequencies are defined as $\beta_i=g_i/W_{31}$, for $i=1,2$, the dimensionless rates $\tilde{W}_{ij}$ are given by the ratios W_{ij}/W_{31} for all values of i and j, and $\tilde{\Delta}_i=\Delta_i/W_{31}$ for $i=1,2$. Finally the collisional excitations rates from lower to higher levels are set equal to zero.

We begin with the analysis of the emission spectra. There can be striking differences between the fluorescence produced by an atom driven by one and by two resonant fields. Curve (*a*) in Fig. 3 illustrates the typical incoherent part of the spectrum produced by the $3\rightarrow1$ spontaneous decay of the V system when the second driving field is turned off ($\beta_2=0$) and the first is moderately large ($\beta_1=1$). As expected, this spectrum is composed of a single peak centered at $\omega=\omega_{31}$ with a full width at half

maximum of the order of unity in the chosen units. The sidebands are beginning to show up but are not yet resolved at the selected field strength. A precise analysis would show small quantitative differences between this spectrum and that of a simple two-level system driven by the same field because of the additional relaxation pathway from level 3 that is built into our model, but the results are substantially similar.

If the second field is turned on and, in particular, if β_2 is sufficiently larger than β_1, the shape of the emission spectrum undergoes major modifications, as shown by curve (*b*) of Fig. 3. By inspection we recognize the following.

(1) The spectrum develops sidebands whose frequency spacing from the central peak is given approximately by $\pm 2(\beta_1^2+\beta_2^2)^{1/2}$ (this empirical observation is supported by the calculations of Sec. V of this paper.

(2) The integrated area under the spectrum of curve (*b*), i.e., the total fluorescence, is smaller than the corresponding area under the spectrum of curve (*a*).

(3) The linewidth of each spectral component of curve (*b*) is much smaller than predicted by the standard theory of resonance fluorescence.

It is not so obvious how to account for these features on the basis of the calculations developed in Sec. II and III (at least not by direct inspection of the formulas); in Sec. V we show that a more convenient representation of the density operator in terms of dressed atomic states[15] paves the way for the analytic derivation of explicit expressions for the shape of the emission spectra, their peak heights and widths, and explains the origin of the features noted in Fig. 3. Here we anticipate that, in resonance, the allowed transitions among these dressed atomic states can generate up to five spectral components; two sidebands are spaced at a distance $\pm 2(\beta_1^2+\beta_2^2)^{1/2}$ from the central peak and two are half as far away from the center. Detailed calculations show that the inner sidebands are usually small for moderate values of β_1, and in fact they are virtually unobservable in the case shown in Fig. 3.

The strong reduction of the integrated area under the spectrum of curve (b) of Fig. 3 is a consequence of a phenomenon called "coherent population trapping" which has already been studied both experimentally and theoretically.[13,14,16,17] In Ref. 16, for example, Gray, Whitley, and Stroud offered a clear experimental demonstration of this effect in a Λ system, and Orriols[17] predicted similar but less pronounced features for a V system, as well. An illustration of this effect is given in Figs. 4(a)–4(d) where we plot the populations of levels 3 and 2 for a V and a Λ system using $\tilde{\Delta}_2=0$ and variable $\tilde{\Delta}_1$. When $\tilde{\Delta}_1=\tilde{\Delta}_2$, the excited state populations, hence the total fluorescence, reach a minimum for both models, which is significantly more pronounced in the case of Fig. 4(c) than in Fig. 4(a). A detailed analysis of this effect

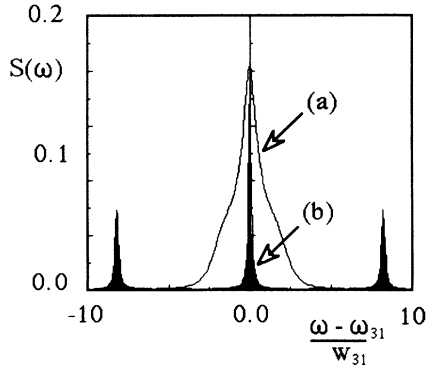

FIG. 3. Curve (*a*), Power spectrum of the spontaneous radiation emitted by the $3\rightarrow 1$ transition for $\tilde{W}_{21}=0.1$, $\tilde{W}_{32}=0.5$, $\tilde{\Delta}_1=0$, $\tilde{\Delta}_2=0$, $\beta_1=1$, and $\beta_2=0$; apart from small quantitative differences this spectrum is very similar to the standard Mollow spectrum; curve (*b*) same as curve (*a*) except that $\beta_2=4$.

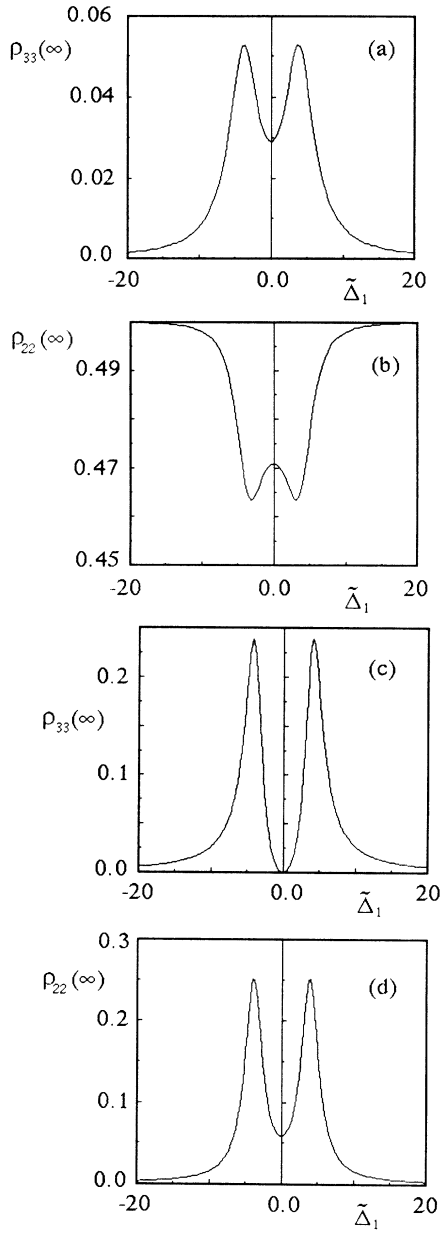

FIG. 4. Dependence of the steady-state populations of level 3 (a) and level 2 (b) upon the detuning parameter $\tilde{\Delta}_1$ for the V model; the parameters are $\tilde{W}_{21}=0.1$, $\tilde{W}_{32}=0$, $\tilde{\Delta}_2=0$, $\beta_1=1$, and $\beta_2=4$. The chosen value of $\tilde{W}_{32}$ minimizes the fluorescence from level 3 when $\tilde{\Delta}_1=0$. (c) and (d) refer to the populations of levels 3 and 2, respectively, for the Λ model; here $\tilde{W}_{21}=0$, $\tilde{W}_{32}=0.5$, $\Delta_2=0$, $\beta_1=1$, and $\beta_2=4$. The chosen value of $\tilde{W}_{21}$ minimizes the fluorescence from level 3 when $\tilde{\Delta}_1=0$.

can be found in Ref. 17. The immediate consequence of population trapping on the spectra is the appearance of dark lines as one sweeps the detuning parameter $\tilde{\Delta}_1$, as shown in Figs. 5(a)–5(c). These are rather well in evidence in the sidebands produced by the $3\rightarrow 1$ transition [Fig. 5(a)], but show up unmistakably in Fig. 5(c) which illustrates a spectral scan for the $3\rightarrow 1$ transition of the Λ model to emphasize the difference with the V system.

The origin of the line narrowing phenomenon is also well explained by the dressed atom picture but an understanding of this effect requires a careful analysis of the entire master equation in the dressed state representation, and for this we must refer the reader to the detailed discussion of Sec. V. This phenomenon originates from the fact that the spontaneous decay rate of each atomic transition in the presence of the driving fields becomes a linear superposition of all decay rates $\tilde{W}_{ij}$ connecting the levels of interest, with weighting factors that depend on the relative magnitudes of the Rabi frequencies. For this reason, and in anticipation of the analytic results of Sec. V, it is interesting to consider the behavior of the spectral features as we vary the key parameters of the theory.

Figure 6(a) illustrates the role of the decay rate $\tilde{W}_{21}$ in affecting the linewidth of the $3\rightarrow 1$ spectrum when β_2/β_1 is sufficiently large; Fig. 6(b) shows the appearance of an additional pair of sidebands separated from the central peak by an amount $\pm(\beta_1^2+\beta_2^2)^{1/2}$. Upon increasing $\tilde{W}_{32}$ these sidebands grow; their magnitude is also sensitive to the size of β_1 and is usually quite small for moderate values of this Rabi frequency. Of course, in general, the decay rates $\tilde{W}_{ij}$ are not adjustable parameters. It should be much easier instead to vary the relative strength of the driving field amplitudes as shown in the simulation of Fig. 7. This three-dimensional plot combines all the effects discussed previously: the narrowing of the central line, the appearance of the inner sidebands, and the population trapping effect (see, in particular, the lowering of the central peak and the emergence and disappearance of the inner sidebands).

A more detailed view of the dependence of the peak heights and linewidths on the Rabi frequency of the second field is shown in Figs. 8 and 9. Here we have selected a fixed and fairly large value of β_1 ($\beta_1=3$). The isolated points are the results of the exact numerical calculations, while the solid lines follow from the asymptotic approximation of Sec. V. The agreement is generally quite satisfactory over the range where the effective Rabi frequency is sufficiently large. An exception is provided

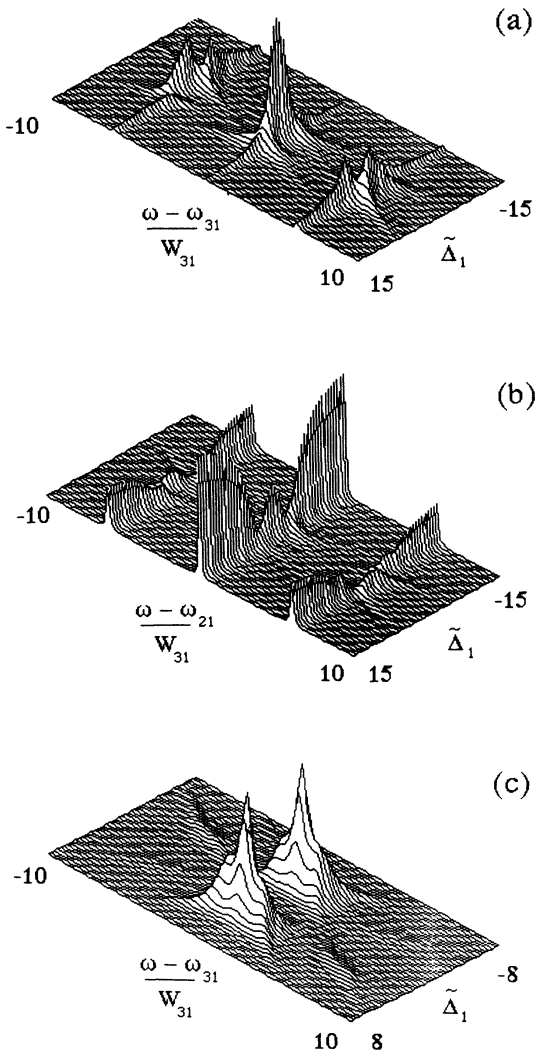

FIG. 5. (a) Emission spectra of the $3\rightarrow 1$ transition and (b) of the $2\rightarrow 1$ transition as functions of $\tilde{\Delta}_1$ for the V model; (c) emission spectra of the $3\rightarrow 1$ transition also as functions of $\tilde{\Delta}_1$ for the Λ model; the parameters of these simulations are $\tilde{W}_{21}=0.1$, $\tilde{W}_{32}=0.5$, $\tilde{\Delta}_2=0$, $\beta_1=1$, and $\beta_2=3$.

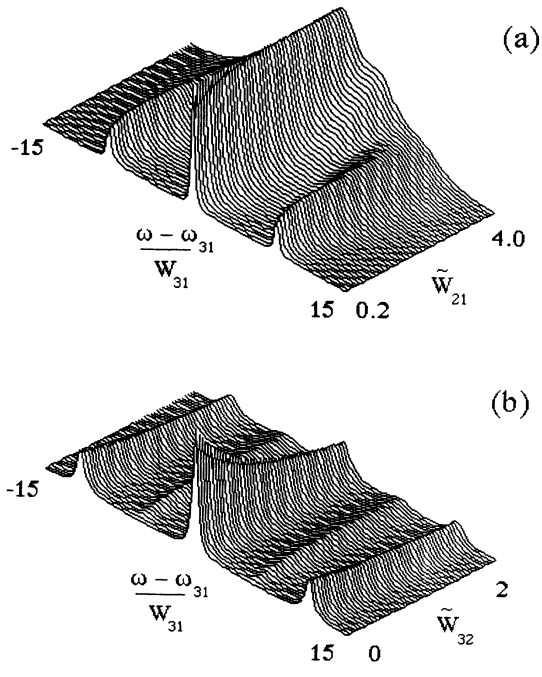

FIG. 6. (a) Emission spectra of the $3\rightarrow 1$ transition as functions of the relaxation rates $\tilde{W}_{21}$ and (b) as functions of $\tilde{W}_{32}$; the parameters of these simulations are $\tilde{\Delta}_1=0$, $\tilde{\Delta}_2=0$, and $\tilde{W}_{32}=0.5$, $\beta_1=1$ and $\beta_2=4$, for (a), and $\tilde{W}_{21}=0.1$, $\beta_1=4$ and $\beta_2=4$, for (b). Each spectrum in (a) has been normalized to unity to put in better evidence the line narrowing effect.

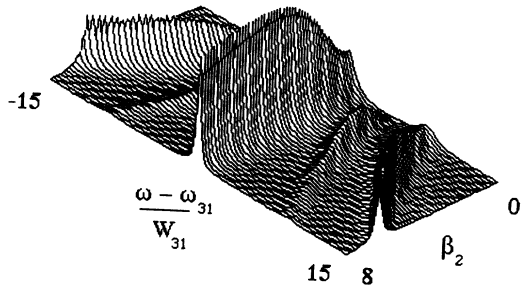

FIG. 7. Emission spectra of the $3\rightarrow 1$ transition as functions of β_2; the parameters are $\tilde{W}_{21}=0.1$, $\tilde{W}_{32}=0.5$, $\tilde{\Delta}_1=0$, $\tilde{\Delta}_2=0$, and $\beta_1=4$.

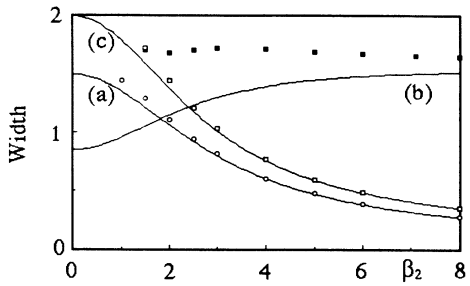

FIG. 9. Dependence of the linewidths of the spectral components of the $3\rightarrow 1$ spectrum upon the Rabi frequency β_2. Curves (a)–(c) represent the widths of the central component, of the $\pm G$ sidebands, and of the $\pm 2G$ sidebands, respectively. The parameters of this simulation are $\tilde{W}_{21}=0.1$, $\tilde{W}_{32}=0.5$, $\beta_1=3$. The isolated points have been calculated using the formulas of Sec. III, the solid lines are plots of the asymptotic results of Sec. V.

by the linewidth data for the inner sidebands which converge more slowly to the corresponding asymptotic values (in part this is due also to systematic errors introduced by the smallness of these spectral components and the consequent importance of the wings of the other peaks).

The absorption spectrum of a weak probe offers additional surprises. Here we focus on a situation where a weak tunable beam, with a carrier frequency close to either ω_{31} or ω_{21}, propagates through the system of driven atoms. We consider first the well-known case where only one driving field is present ($\beta_1=1, \beta_2=0$). Figure 10 shows the absorption spectrum of the $3\rightarrow 1$ resonance; this as the standard shape predicted by Mollow, apart from small quantitative differences resulting from the extra decay pathways included in this model. We note the expected appearance of frequency intervals where the probe can be amplified instead of being absorbed. Figures 11 and 12 show the absorption spectra of the $1\rightarrow 2$ and $1\rightarrow 3$ transitions when both fields are present for different values of the second driving field amplitude. The absorption spectra of both transitions have a fairly complex structure with alternating regions of absorption and gain depending on the strength of the second field

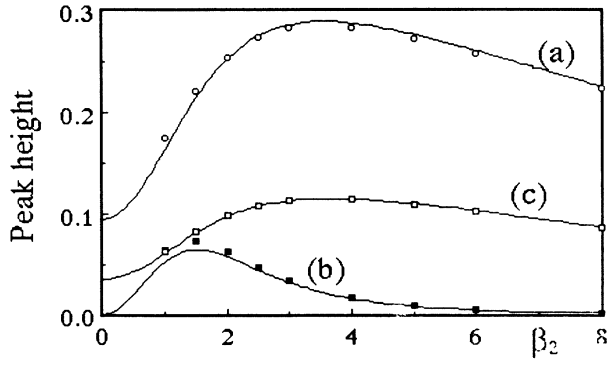

FIG. 8. Dependence of the peak heights of the spectral components of the $3\rightarrow 1$ spectrum upon the Rabi frequency β_2. Curves (*a*), (*b*), and (*c*) represent the peaks of the central component, of the $\pm G$ sidebands, and of the $\pm 2G$ sidebands, respectively. The parameters of this simulation are $\tilde{W}_{21}=0.1$, $\tilde{W}_{32}=0.5$, $\beta_1=3$. The isolated points have been calculated using the formulas of Sec. III, the solid lines are plots of the asymptotic results of Sec. V.

and the relaxation rates $\tilde{W}_{21}$ and $\tilde{W}_{31}$. It is interesting to note, for example, that the gain region for small values of β_2 and $\tilde{W}_{21}=0.1$ [Fig. 11(a)] collapses into an absorbing one for larger relaxation rates [Fig. 12(a)].

A more interesting situation emerges as we vary the strength of β_1 by keeping the ratio β_2/β_1 constant and smaller than unity. We anticipate here that, according to the asymptotic calculations developed in Sec. V, the weak probe should experience gain over the entire frequency range of the transition that is being probed. Here we show that this behavior is accessible even with relatively small Rabi frequencies. The transition from absorption to gain over the entire frequency range of the $1\rightarrow 2$ transition is illustrated in Figs. 13(a) and 13(b). This response is very different from that of the traditional two-level system where gain regions, if they exist, are always accompanied by absorption domains. Thus, in the case of Fig. 13(b), the three-level atoms acquire many of the properties of an ordinary active medium. This interesting effect is best explained with the help of the dressed atom model and the asymptotic calculations carried out in Sec. V to which we refer the reader for a more complete discussion.

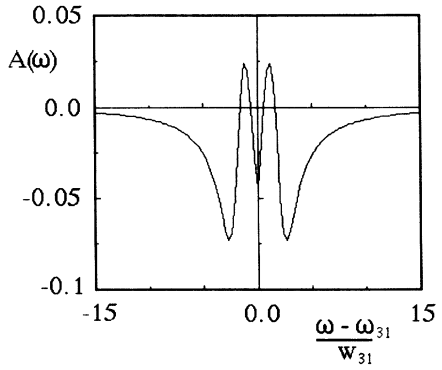

FIG. 10. Absorption spectrum of a weak probe around the ω_{31} resonance. The parameters of this simulation are $\tilde{W}_{21}=1$, $\tilde{W}_{32}=0.5$, $\tilde{\Delta}_1=0$, $\tilde{\Delta}_2=0$, $\beta_1=1$, and $\beta_2=0$.

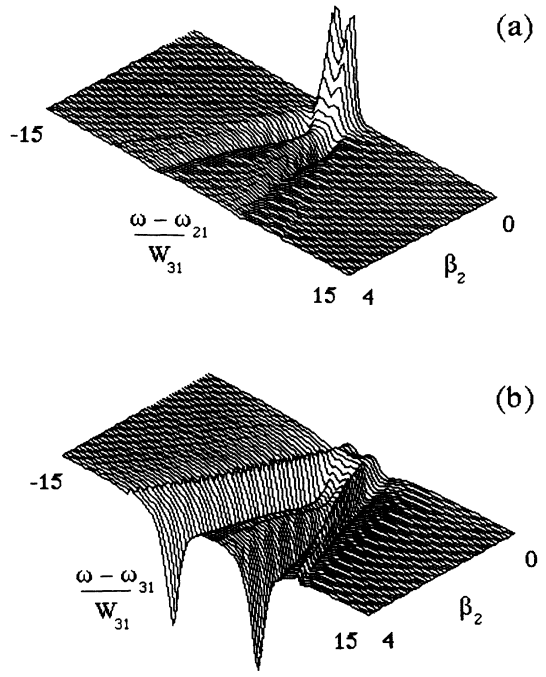

FIG. 11. Absorption spectra of a weak probe around (a) the ω_{21} resonance, and (b) the ω_{31} resonance for different values of β_2. The parameters are $\tilde{W}_{21}=0.1$, $\tilde{W}_{32}=0.5$, $\tilde{\Delta}_1=0$, $\tilde{\Delta}_2=0$, and $\beta_1=1$.

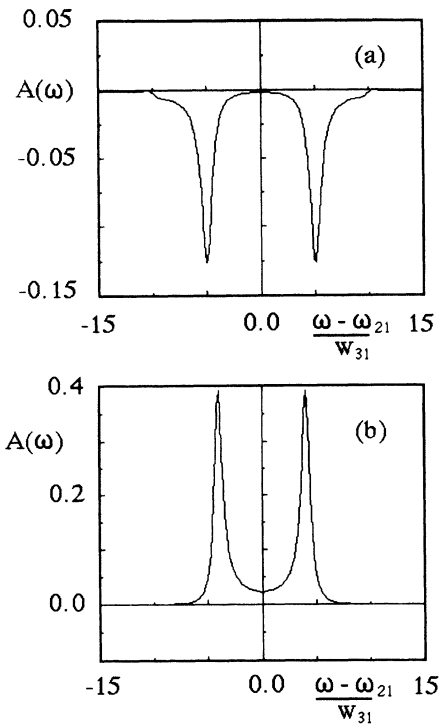

FIG. 13. Absorption spectrum of a weak probe around the ω_{21} resonance for $\tilde{W}_{21}=0.1$, $\tilde{W}_{32}=0.5$, $\tilde{\Delta}_1=0$, $\tilde{\Delta}_2=0$, $\beta_1=4$ and (a) $\beta_2=3$ and (b) $\beta_2=1$.

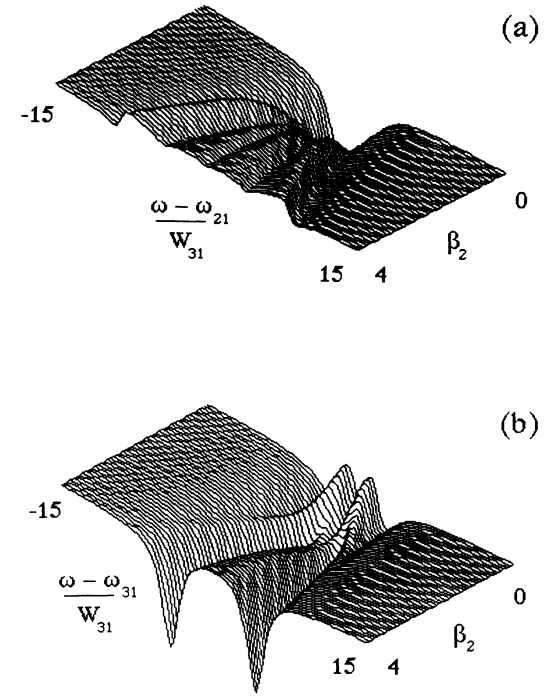

FIG. 12. Same as Fig. 11 except that here $\tilde{W}_{21}=1.0$.

V. ANALYTIC CALCULATION OF THE SPECTRA IN THE HIGH EFFECTIVE FIELD LIMIT

The procedure outlined in Secs. II and III offers a convenient numerical access to numerous interesting properties of the three-level system, but it suffers from a major drawback: the results cannot be visualized in any simple way because the operating physical mechanisms are hidden by the algebraic complexity of the final expressions. In a way, this is the same problem one would face in describing the coherence properties of the electromagnetic field using the energy representation. It is possible to do so, of course, but there are more natural representations for this purpose. The difficulty, in our case, is that the energy representation hides the strong correlations that are induced among the three atomic levels by the coherent driving fields.

In this section we show that a convenient set of dressed atomic states[15] paves the way to a much more natural description of the atomic dynamics and that, in the limit of a strong effective Rabi frequency, this allows the calculation of the required correlation functions and the spectra in closed analytic form. The immediate payoff of this procedure is that explicit expressions for the line shapes, linewidths, and peak heights become available, so that one can trace the origin of the behaviors illustrated by the numerical work of Sec. IV almost at a glance.

The only problem is that this method is useful only as an asymptotic approximation, so that the numerical calculations of the preceding section are really unavoidable for arbitrary values of the parameters. Hence, the pro-

cedure outlined in Secs. II and III and the one described below are complementary to one another. We should also add that the dressed atomic states formalism appears to be quite promising for a number of different applications; as shown in Appendix A, for example, it can be extended easily to include situations where the driving fields are quantized and it should be useful to study a broader class of problems that can be handled in the semiclassical approximation.

The underlying notion is common to every situation where an important part of the interaction Hamiltonian can be diagonalized exactly. Here, as we show, the interaction Hamiltonian (2.3) can be diagonalized easily, while the irreversible mechanism leading to the atomic decay and dephasing can be handled approximately in a sense that will be made more precise in our discussion. In order to minimize the algebraic labor we limit our considerations to the case of a resonant interaction ($\tilde{\Delta}_1=\tilde{\Delta}_2=0$) and we study only the emission spectrum of the $3\rightarrow 1$ transition. For the $2\rightarrow 1$ emission spectrum and for the absorption spectrum we only quote the relevant results.

Thus, consider the interaction Hamiltonian (2.3) with $\tilde{\Delta}_1=\tilde{\Delta}_2=0$. Consider the dressed atomic states[15]

$$|r\rangle=(\cos\theta)|2\rangle-(\sin\theta)|3\rangle\ , \tag{5.1a}$$

$$|s\rangle=\frac{1}{\sqrt{2}}[(\sin\theta)|2\rangle+(\cos\theta)|3\rangle+|1\rangle]\ , \tag{5.1b}$$

$$|t\rangle=\frac{1}{\sqrt{2}}[(\sin\theta)|2\rangle+(\cos\theta)|3\rangle-|1\rangle]\ , \tag{5.1c}$$

with

$$\tan\theta=\frac{g_2}{g_1}\ . \tag{5.2}$$

These states are eigenstates of H_1', i.e.,

$$H_1'|r\rangle=0\ , \tag{5.3a}$$

$$H_1'|s\rangle=\hbar G|s\rangle\ , \tag{5.3b}$$

$$H_1'|t\rangle=-\hbar G|t\rangle\ , \tag{5.3c}$$

and

$$G=(g_1^2+g_2^2)^{1/2} \tag{5.4}$$

represents the effective applied Rabi frequency. Because of the diagonal nature of H_1' in this representation, the new matrix L, which is responsible for the atomic dynamics, contains the effective Rabi frequency along the main diagonal and is zero elsewhere. The irreversible decay process breaks this symmetry. However, if the effective Rabi frequency is sufficiently large, it is possible to introduce an accurate approximation that allows considerable analytic progress. In fact, in our case we show that, while G must be large for this approximation to hold, no restrictions are posed on the individual magnitudes of the two Rabi frequencies g_1 and g_2.

We consider again the master equation in the interaction picture

$$\frac{\partial\rho'}{\partial t}=-\frac{i}{\hbar}[H_1',\rho']+\Lambda\rho'\ . \tag{5.5}$$

The reversible part of Eq. (5.5) in the dressed state representation takes a very simple form owing to the fact that the states (5.1) are exact eigenstates of H_1'. Thus we have

$$\left[\frac{\partial}{\partial t}\right]_{\rm rev}\begin{bmatrix}\rho'_{st}\\ \rho'_{sr}\\ \rho'_{rt}\\ \rho'_{ss}\\ \rho'_{tt}\end{bmatrix}=\begin{bmatrix}-2iG\rho'_{st}\\ -iG\rho'_{sr}\\ -iG\rho'_{rt}\\ 0\\ 0\end{bmatrix}\ . \tag{5.6}$$

Again, we have the trace condition

$$\rho'_{rr}=1-\rho'_{ss}-\rho'_{tt} \tag{5.7}$$

and the Hermitian symmetry

$$\rho'_{rs}=(\rho'_{sr})^*,\quad \rho'_{\rm tr}=(\rho'_{rt})^*,\quad \rho'_{ts}=(\rho'_{st})^*\ . \tag{5.8}$$

It is interesting to observe that of the eight independent components $\rho'_{\mu\nu}$ of the density operator (we use Greek indices to denote the matrix elements in the dressed state representation, and Latin indices for the standard energy representation) two are associated with the frequency $+iG$, two with $-iG$, two with zero frequency, and one each with $\pm 2iG$. These groupings reflect the various contributions of the density operator to the five spectral components. For this reason we have chosen to order the matrix elements as shown in Eq. (5.6) beginning with the $+2G$ sideband of the spectrum.

The penalty one pays for using this representation is that the irreversible part of the master equation becomes very complicated. In fact, the original irreversible part of the master equation is

$$\left[\frac{\partial}{\partial t}\right]_{\rm irrev}\rho'_{ij}=\sum_{p,q}\Lambda_{ijpq}\rho'_{pq}\ , \tag{5.9}$$

where Λ_{ijpq} are the various decay rates that appear explicitly in Eq. (2.10). From the transformation equation between the two pictures

$$\rho'_{\mu\nu}=\sum_{i,j}\langle\mu|i\rangle\rho'_{ij}\langle j|\nu\rangle \tag{5.10}$$

it is easy to obtain

$$\left[\frac{\partial}{\partial t}\right]_{\rm irrev}\rho'_{\mu\nu}=\sum_{\sigma,\tau}\left[\sum_{i,j,p,q}\langle\mu|i\rangle\langle j|\nu\rangle\langle p|\sigma\rangle\langle\tau|q\rangle\Lambda_{ijpq}\right]\rho'_{\sigma\tau}=\sum_{\sigma,\tau}\Gamma_{\mu\nu\sigma\tau}\rho'_{\sigma\tau}\ , \tag{5.11}$$

where the transformation matrix elements $\langle \mu | i \rangle$ can be read immediately from Eq. (5.1). The explicit construction of Eq. (5.11) for each matrix element of ρ' is an enormous chore which is ideally suited for symbolic logic programs (this is, in fact, what we have done in our work). The resulting list of damping rates $\Gamma_{\mu\nu\sigma\tau}$ is too long to be included in this paper even when allowance is made for various symmetry relations.

We now focus on the derivation of an expression for the fluorescence spectrum in the limit in which G is much larger than all the relaxation rates. Following a procedure that accounts for the approach to steady state and for the response of the system around steady state with an accuracy of order $1/G$, we introduce the usual vector ψ with components

$$\psi_1=\rho'_{st},\quad \psi_2=\rho'_{sr},\quad \psi_3=\rho'_{rt},\quad \psi_4=\rho'_{ss}\ ,$$
$$\psi_5=\rho'_{tt},\quad \psi_6=\rho'_{rs},\quad \psi_7=\rho'_{\mathrm{tr}},\quad \psi_8=\rho'_{ts}\ , \tag{5.12a}$$

$$\rho'_{rr}=1-\rho'_{ss}-\rho'_{tt}=1-\psi_4-\psi_5\ . \tag{5.12b}$$

This vector is a solution of the linear equation

$$\frac{\partial}{\partial t}\psi=L\psi+\mathbf{I} \tag{5.13}$$

and, in steady state, it takes the form

$$\psi(\infty)=-L^{-1}\mathbf{I}\ . \tag{5.14}$$

Normally we would solve Eq. (5.14) by numerical techniques. Because, however, we are interested in an approximate asymptotic solution, we note that in steady state the off-diagonal elements of ρ' are of the order of $1/G$, while the diagonal elements are of the order of unity [see Eqs. (5.6) and (5.11)]. In this limit the dominant matrix elements are

$$\psi_4(\infty)=\psi_5(\infty)\equiv\psi_\infty=-\frac{\Gamma_{ssrr}}{\Gamma_{sstt}+\Gamma_{ssss}-2\Gamma_{ssrr}}=\frac{W_{32}\frac{1}{2}\sin^4\theta+W_{31}\frac{1}{2}\sin^2\theta+W_{21}\frac{1}{2}\cos^2\theta}{W_{32}(\frac{1}{2}\cos^4\theta+\sin^4\theta)+W_{31}\sin^2\theta+W_{21}\cos^2\theta}\ . \tag{5.15}$$

Note that if $W_{32}=0$ we have

$$\psi_\infty=\tfrac{1}{2},\quad \rho'_{rr}=0\ . \tag{5.16}$$

We now define the deviation from steady state

$$\delta\psi=\psi(t)-\psi(\infty)\ , \tag{5.17}$$

which satisfies the equation

$$\frac{\partial}{\partial t}\delta\psi(t)=L\delta\psi(t)\ . \tag{5.18}$$

Of course Eq. (5.18) is just as complicated to solve as the original equation (5.13). In the asymptotic limit of interest, however, we can replace the matrix L in the fluctuation equation (5.18) with a block-diagonal approximation L_0 (see below) which is accurate up to corrections of order $1/G$. This step allows the analytic calculation of the spectrum.

In order to understand the nature of this approximation we summarize the essential steps in Appendix B. The result of this procedure is a fluctuation equation of the form

$$\frac{\partial}{\partial t}\delta\psi(t)=L_0\delta\psi(t) \tag{5.19}$$

or, in terms of the original vector ψ [see Eq. (5.17)]

$$\frac{\partial}{\partial t}\psi(t)=L_0\psi(t)+\mathbf{I}_\infty\ , \tag{5.20}$$

where

$$\mathbf{I}_\infty=-L_0\psi(\infty)\ . \tag{5.21}$$

The diagonal blocks of L_0, denoted by $(L_0)_i$ are given explicitly by

$$(L_0)_1=\Gamma_{stst}-2iG\ , \tag{5.22a}$$

$$(L_0)_2=\begin{bmatrix}\Gamma_{srsr}-iG & \Gamma_{srrt}\\ \Gamma_{stsr} & \Gamma_{rtrt}-iG\end{bmatrix}, \tag{5.22b}$$

$$(L_0)_3=\begin{bmatrix}\Gamma_{ssss}-\Gamma_{ssrr} & \Gamma_{sstt}-\Gamma_{ssrr}\\ \Gamma_{ttss}-\Gamma_{ttrr} & \Gamma_{tttt}-\Gamma_{ttrr}\end{bmatrix}, \tag{5.22c}$$

$$(L_0)_4=\begin{bmatrix}\Gamma_{rsrs}+iG & \Gamma_{rstr}\\ \Gamma_{trrs} & \Gamma_{trtr}+iG\end{bmatrix}, \tag{5.22d}$$

$$(L_0)_5=\Gamma_{tsts}+2iG\ . \tag{5.22e}$$

In view of the symmetry relations among the decay rates it is convenient to let

$$\Gamma_{stst}=\Gamma_{tsts}=\gamma_1\ ,$$
$$\Gamma_{srsr}=\Gamma_{rtrt}=\Gamma_{rsrs}=\Gamma_{trtr}=\gamma_2\ ,$$
$$\Gamma_{srrt}=\Gamma_{rtsr}=\Gamma_{rstr}=\Gamma_{trrs}=\gamma_3\ , \tag{5.23}$$
$$\Gamma_{ssss}-\Gamma_{ssrr}=\Gamma_{tttt}-\Gamma_{ttrr}=\gamma_4\ ,$$
$$\Gamma_{sstt}-\Gamma_{ssrr}=\Gamma_{ttss}-\Gamma_{ttrr}=\gamma_5\ .$$

The only nonzero elements of the vector $\mathbf{I}_\infty$ (to order $1/G$) are

$$I_{\infty 4}=I_{\infty 5}=\Gamma_{ssrr}=W_{32}\tfrac{1}{2}\sin^4\theta+W_{31}\tfrac{1}{2}\sin^2\theta+W_{21}\tfrac{1}{2}\cos^2\theta\ . \tag{5.24}$$

At this point the procedure for the calculation of the spectrum evolves along the lines described in Sec. III. The solution of Eq. (5.20) in Laplace space is

$$\hat{\boldsymbol{\psi}}(z)=M^0(z)\boldsymbol{\psi}(t_0)+\frac{1}{z}M^0(z)\mathbf{I}_\infty \ , \tag{5.25}$$

where

$$M^0(z)=(z-L_0)^{-1} \ . \tag{5.26}$$

For simplicity we consider only the emission process for the $3\rightarrow 1$ transition so that

$$P^{(+)}=a_1^\dagger a_3, \quad P^{(-)}=a_3^\dagger a_1 \ . \tag{5.27}$$

As usual, we need the single-time average

$$\langle P^{(-)}(t_1)\rangle=\mathrm{Tr}[\rho'(t_1)a_3^\dagger a_1]\exp(i\omega_{31}t_1) \ . \tag{5.28}$$

In terms of dressed states we have

$$a_3^\dagger a_1|r\rangle=0 \ , \tag{5.29a}$$

$$a_3^\dagger a_1|s\rangle=\tfrac{1}{2}(\cos\theta)(|s\rangle+|t\rangle)-\frac{1}{\sqrt{2}}(\sin\theta)|r\rangle \ , \tag{5.29b}$$

$$a_3^\dagger a_1|t\rangle=-\tfrac{1}{2}(\cos\theta)(|s\rangle+|t\rangle)+\frac{1}{\sqrt{2}}(\sin\theta)|r\rangle \ , \tag{5.29c}$$

so that, in Laplace space, it follows that

$$\langle \hat{P}^{(-)}(z)\rangle=\tfrac{1}{2}(\cos\theta)[\hat{\psi}_4(z_1)+\hat{\psi}_1(z_1)-\hat{\psi}_8(z_1)-\hat{\psi}_5(z_1)]-\frac{1}{\sqrt{2}}(\sin\theta)[\hat{\psi}_2(z_1)-\hat{\psi}_7(z_1)] \ , \tag{5.30}$$

where

$$z_1=z-i\omega_{31} \tag{5.31}$$

and the components of $\boldsymbol{\psi}$ are defined according to Eqs. (5.12). After replacing $\hat{\psi}_i(z_1)$ by the appropriate expressions [see Eq. (5.25)] in terms of $\psi_i(t_0)$ we only need to cast the various $\psi_i(t_0)$ in the form of expectation values and to carry out the standard replacements required by the regression theorem. Thus, for example, we have

$$\begin{aligned}\psi_1(t_0)\rightarrow\mathrm{Tr}[\rho(t_0)\overline{|t\rangle\langle s|}a_1^\dagger a_3]&=\mathrm{Tr}[\rho'(t_0)|t\rangle\langle s|\overline{a_1^\dagger a_3}]\\&=\exp(-i\omega_{31}t_0)\langle s|a_1^\dagger a_3\rho'(t_0)|t\rangle\\&=\exp(-i\omega_{31}t_0)\left[\tfrac{1}{2}(\cos\theta)(\rho'_{st}+\rho'_{tt})-\frac{1}{\sqrt{2}}(\sin\theta)\rho'_{rt}\right] \ ,\end{aligned} \tag{5.32}$$

where the overbars indicate that the operators are in the interaction picture. Similar expressions hold for the remaining components of $\boldsymbol{\psi}(t_0)$. Note that in the stationary limit of the off-diagonal elements of $\rho'_{\mu\nu}$ vanish and the only nonzero elements are

$$\rho'_{ss}=\rho'_{tt}=\psi_\infty \tag{5.33}$$

as given by Eq. (5.15). In this way, Eq. (5.32) becomes

$$\psi_1(t_0\rightarrow\infty)=\exp(-i\omega_{31}t_0)\tfrac{1}{2}(\cos\theta)\psi_5(\infty)+O(1/G) \tag{5.34}$$

and the other matrix elements can be handled in a similar way. The result of these manipulations is the correlation function

$$\langle \hat{P}^{(-)}(z)P^{(+)}(\infty)\rangle=\tfrac{1}{4}(\cos^2\theta)\psi_\infty(M^0_{11}+M^0_{44}-M^0_{54}+M^0_{55}+M^0_{88})+\tfrac{1}{2}(\sin^2\theta)(1-2\psi_\infty)(M^0_{22}+M^0_{77}) \ . \tag{5.35}$$

At this point we need to calculate the explicit expressions for the matrix elements M^0_{ij}. This task is made easy by the fact that the first and last blocks of the M^0 matrix are trivial, while the remaining three blocks have the generic form

$$\begin{bmatrix}a & b\\ b & a\end{bmatrix}\underset{\text{inverse}}{\rightarrow}\frac{1}{a^2-b^2}\begin{bmatrix}a & -b\\ -b & a\end{bmatrix} \ . \tag{5.36}$$

After a few simple calculations Eq. (5.35) becomes

$$\begin{aligned}\langle \hat{P}^{(-)}(z)P^{(+)}(\infty)\rangle=&\tfrac{1}{4}(\cos^2\theta)\psi_\infty\left[\frac{1}{z_1-\gamma_1+2iG}+\frac{2}{z_1-\gamma_4+\gamma_5}+\frac{1}{z_1-\gamma_1-2iG}\right]\\&+\tfrac{1}{2}(\sin^2\theta)(1-2\psi_\infty)\left[\frac{z_1-\gamma_2+iG}{(z_1-\gamma_2+iG)^2-\gamma_3^2}+\frac{z_1-\gamma_2-iG}{(z_1-\gamma_2-iG)^2-\gamma_3^2}\right]\end{aligned} \tag{5.37}$$

and the emission spectrum is given by

$$S(\omega)=\mathrm{Re}\langle \hat{P}^{(-)}(z)P^{(+)}(\infty)\rangle|_{z=i(\omega-\omega_{31})} . \tag{5.38}$$

For convenience we list the set of constants that are needed to discuss this result

$$\gamma_1=-W_{32}\tfrac{1}{4}(\cos^2\theta)(1+\cos^2\theta)-W_{31}\tfrac{3}{4}\cos^2\theta - W_{21}\tfrac{3}{4}\sin^2\theta , \tag{5.39a}$$

$$\gamma_2=-W_{32}\tfrac{1}{4}[1+(\sin^2\theta)(1+2\cos^2\theta)] - W_{31}\tfrac{1}{4}(1+\sin^2\theta)-W_{21}\tfrac{1}{4}(1+\cos^2\theta) , \tag{5.39b}$$

$$\gamma_3=-W_{32}\tfrac{1}{2}\sin^2\theta\cos^2\theta , \tag{5.39c}$$

$$\gamma_4=-W_{32}(\tfrac{1}{4}\cos^2\theta+\tfrac{1}{4}\cos^4\theta+\tfrac{1}{2}\sin^4\theta) - W_{31}\tfrac{1}{4}(1+\sin^2\theta)-W_{21}\tfrac{1}{4}(1+\cos^2\theta) , \tag{5.39d}$$

$$\gamma_5=W_{32}\tfrac{1}{2}\sin^2\theta(\tfrac{1}{2}\cos^2\theta-\sin^2\theta)+W_{31}(\tfrac{1}{4}\cos^2\theta-\tfrac{1}{2}\sin^2\theta) + W_{21}(\tfrac{1}{4}\sin^2\theta-\tfrac{1}{2}\cos^2\theta) . \tag{5.39e}$$

The main features of the spectrum whose analytic representation is given by Eq. (5.38) can be summarized as follows.

(1) In general, the emission spectrum of the $3\rightarrow1$ transition is composed of five contributions. One is centered at the transition frequency ω_{31} and has a Lorentzian shape, two sidebands are removed by an amount $\pm G$ from the central peak, and two additional Lorentzian sidebands are located $\pm 2G$ away from the central peak. The outermost sidebands are the ones that also appear in the Mollow spectrum of a strongly driven two-level atom. The inner sidebands are instead a feature of the three-level system, although they disappear if the rate of decay of the $3\rightarrow2$ transition approaches zero because their weighting factor is proportional to W_{32}.

(2) The peak heights of the central component and of the outer sidebands are given by

$$P(0)=\tfrac{1}{4}(\cos^2\theta)\frac{2}{\gamma_5-\gamma_4}\psi_\infty , \tag{5.40a}$$

$$P(\pm2G)=\tfrac{1}{4}(\cos^2\theta)\frac{1}{|\gamma_1|}\psi_\infty , \tag{5.40b}$$

respectively, and their ratio is

$$\frac{P(0)}{P(\pm2G)}=\frac{W_{32}\frac{1}{2}(\cos^2\theta)(1+\cos^2\theta)+W_{31}\frac{3}{2}\cos^2\theta+W_{21}\frac{3}{2}\sin^2\theta}{W_{32}\frac{1}{2}\cos^2\theta+W_{31}\frac{1}{2}\cos^2\theta+W_{21}\frac{1}{2}\sin^2\theta} . \tag{5.41}$$

In the limit $W_{32}\rightarrow0$ this ratio becomes equal to 3, as in the case of the standard Mollow spectrum.

(3) The full widths at half height of the central component and of the outer sidebands are given by

$$\Delta\omega(0)=2(\gamma_5-\gamma_4)=W_{32}\cos^2\theta+W_{31}\cos^2\theta+W_{21}\sin^2\theta , \tag{5.42a}$$

$$\Delta\omega(\pm2G)=2|\gamma_1|=W_{32}\tfrac{1}{2}(\cos^2\theta)(1+\cos^2\theta) + W_{31}\tfrac{3}{2}\cos^2\theta+W_{21}\tfrac{3}{2}\sin^2\theta , \tag{5.42b}$$

respectively. Their ratio, in the limit $W_{32}\rightarrow0$ also approaches the value of the Mollow spectrum. Equations (5.42) confirm the numerical findings with regard to the line narrowing (or broadening) phenomenon. As g_2 becomes progressively larger than g_1, the linewidths are dominated by the relaxation rate W_{21}. Hence if $W_{21}\ll W_{31}$ eventually the spectrum becomes narrower, or vice versa in the opposite limit. Thus this curious phenomenon is the result of a mixing effect produced by two driving fields which assign to the spontaneous decay rate of the $3\rightarrow1$ transition spontaneous contributions pertaining to the other atomic decay processes.

(4) The spectral shape of the inner sidebands is not Lorentzian. Inclusive of the weighting factor, this is given by the more complicated expression

$$S^{\pm G}=\tfrac{1}{2}\sin^2\theta\frac{W_{32}\frac{1}{2}\cos^4\theta}{W_{32}(\frac{1}{2}\cos^4\theta+\sin^4\theta)+W_{31}\sin^2\theta+W_{21}\cos^2\theta}|\gamma_2|\frac{\gamma_2^2-\gamma_3^2+(\omega-\omega_{31}\pm G)^2}{[\gamma_2^2-\gamma_3^2-(\omega-\omega_{31}\pm G)^2]^2+4\gamma_2^2(\omega-\omega_{31}\pm G)^2} \tag{5.43}$$

and its full width at half maximum takes the form

$$\Delta\omega(\pm2G)=2\{[4\gamma_2^4+(\gamma_2^2-\gamma_3^2)^2]^{1/2}-2\gamma_3^2\}^{1/2} . \tag{5.44}$$

Note that, as already mentioned, the weight of the inner sidebands is controlled by W_{32} and that these spectral components disappear in the limit $W_{32}\rightarrow0$.

For the $2\rightarrow1$ spectrum one can easily derive the corresponding results. Again we find a five-peak spectrum in resonance. The central peak has the shape

$$S_{21}^{(0)}=\tfrac{1}{4}(\sin^2\theta)\psi_\infty\frac{2(\gamma_5-\gamma_4)}{(\gamma_5-\gamma_4)^2+(\omega-\omega_{21})^2} , \tag{5.45}$$

with a peak value

$$S_{21}^{(0)}(\max)=\tfrac{1}{4}(\sin^2\theta)\psi_\infty\frac{2}{\gamma_5-\gamma_4} \tag{5.46a}$$

and full width at half maximum

$$\Delta\omega(0)=2(\gamma_5-\gamma_4) . \tag{5.46b}$$

The outer sidebands are removed from the center of the spectrum by $\pm 2G$. They have a Lorentzian shape

$$S_{21}^{(\pm 2G)}(\omega)=\tfrac{1}{4}(\sin^2\theta)\psi_\infty \frac{|\gamma_1|}{\gamma_1^2+(\omega-\omega_{21}\pm 2G)^2} , \quad (5.47)$$

a peak height

$$S_{21}^{(\pm 2G)}(\max)=\tfrac{1}{4}(\sin^2\theta)\frac{\psi_\infty}{|\gamma_1|} , \quad (5.48a)$$

and full width at half maximum

$$\Delta\omega(2G)=2|\gamma_1| . \quad (5.48b)$$

The inner sidebands do not have a Lorentzian shape. Their spectrum is given instead by

$$S_{21}^{(\pm 2G)}(\omega)=\tfrac{1}{2}(\cos^2\theta)(1-2\psi_\infty)\frac{|\gamma_2|[\gamma_2^2-\gamma_3^2+(\omega-\omega_{21}\pm G)^2]}{[\gamma_2^2-\gamma_3^2-(\omega-\omega_{21}\pm G)^2]^2+4\gamma_2^2(\omega-\omega_{21}\pm G)^2} . \quad (5.49)$$

The peak height is

$$S_{21}^{(\pm G)}(\max)=\tfrac{1}{2}(\cos^2\theta)(1-2\psi_\infty)\frac{|\gamma_2|}{|\gamma_2^2-\gamma_3^2|} \quad (5.50a)$$

and the full width at half maximum is

$$\Delta\omega(G)=2\{[4\gamma_3^4+(\gamma_2^2-\gamma_3^2)^2]^{1/2}-2\gamma_3^2\}^{1/2} . \quad (5.50b)$$

Similar calculations can be developed to describe the asymptotic behavior of the absorption spectrum. In this case a surprising fact emerges. Consider, for example, the results of this calculation for the absorption lines of the $1\rightarrow 3$ and $1\rightarrow 2$ transitions which are given, respectively, by

$$A_{31}(\omega)=\frac{\sin^2\theta}{4}[\rho'_{rr}(\infty)-\rho'_{tt}(\infty)]\left[\frac{|\gamma_2+\gamma_3|}{(\omega-\omega_{31}-G)^2+(\gamma_2+\gamma_3)^2}+\frac{|\gamma_2-\gamma_3|}{(\omega-\omega_{31}-G)^2+(\gamma_2-\gamma_3)^2}+\frac{|\gamma_2+\gamma_3|}{(\omega-\omega_{31}+G)^2+(\gamma_2+\gamma_3)^2}+\frac{|\gamma_2-\gamma_3|}{(\omega-\omega_{31}+G)^2+(\gamma_2-\gamma_3)^2}\right] , \quad (5.51a)$$

$$A_{21}(\omega)=\frac{\cos^2\theta}{4}[\rho'_{rr}(\infty)-\rho'_{tt}(\infty)]\{\} , \quad (5.51b)$$

where $\rho'_{rr}(\infty)$ and $\rho'_{tt}(\infty)$ are the steady-state populations of the dressed states r and t and the curly brackets of Eq. (5.51b) stand for the same expression within the large parentheses Eq. (5.51a) after replacing ω_{31} with ω_{21}. We see, by inspection, the following.

(i) The only spectral features, to order $1/G$, correspond to the $\pm G$ sidebands; the others are of higher order and, in the large G limit, become negligible.

(ii) The expressions in the large parentheses of Eq. (5.51) are positive definite, so that the sign of the absorption spectrum is determined for all values of ω by the steady-state population difference $\rho'_{rr}(\infty)-\rho'_{tt}(\infty)$. In particular, if this quantity is positive, i.e., if

$$W_{32}(\cos^2\theta-\sin^2\theta)\geq W_{31}\sin^2\theta+W_{21}\cos^2\theta \quad (5.52a)$$

or

$$\left[\frac{g_2}{g_1}\right]^2\leq\frac{\tilde{W}_{32}-\tilde{W}_{21}}{1+\tilde{W}_{32}} \quad (5.52b)$$

the atoms amplify the probe radiation, while if it is negative they absorb it. This result is unlike the corresponding amplification process of a weak probe predicted by Mollow because the response of this system, under condition (5.52), is of the same type over the entire frequency range.

The implications of this result are especially clear in the limit in which $\tan\theta=g_2/g_1\rightarrow 0$. In fact, in this limit Eq. (5.52b) implies $W_{32}\geq W_{21}$ and this is precisely the situation that favors the accumulation of population in level 2 under steady-state conditions and produces gain at the $2\rightarrow 1$ transition. There is more, however, because the existence of a steady-state population inversion between the dressed states r and t implies simultaneous inversion between the atomic levels 2-1 and 3-1, as one can easily verify by converting $\rho'_{rr}(\infty)-\rho'_{tt}(\infty)$ into the corresponding combination of matrix elements in the original representation. Nevertheless, the origin of the amplification is not just a trivial consequence of amplified spontaneous emission in the presence of population inversion because the maximum gain does not occur at exactly the transition frequency ω_{21} (or ω_{31}) but at $\omega_{21}\pm G$ (or $\omega_{31}\pm G$). An example of this behavior is shown in Fig. 14 where we compare the exact numerical solutions (dots) with the graphical display of Eq. (5.51a) (solid line).

VI. CONCLUSIONS

This study completes and extends a number of earlier investigations[13–19] on the response of three-level atoms

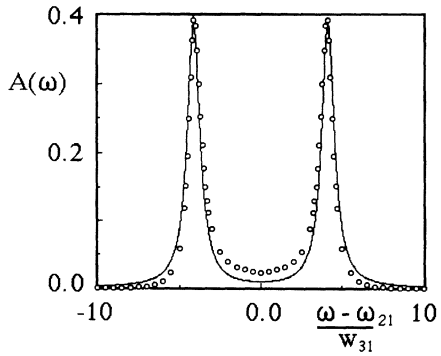

FIG. 14. A fit between the exact absorption spectrum of a weak probe around the ω_{21} resonance (open circles) and the asymptotic approximation of Sec. V (solid curve) for $\tilde{W}_{21}=0.1$, $\tilde{W}_{32}=0.5$, $\tilde{\Delta}_1=0$, $\tilde{\Delta}_2=0$, $\beta_1=4$, and $\beta_2=1$.

to external driving fields. It has been known for some time that multilevel atoms can display a much broader range of effects than their two-level counterparts as a result of the coherence induced among the states by the radiation, and the interference effects that can produce unexpected and sometimes counterintuitive behaviors (e.g., coherent population trapping). In this work we have focused mainly on the properties of spontaneous emission from a V-model atom and on the shape of the absorption spectrum of a weak probe passing through the collection of driven atoms.

The most interesting consequence of the presence of two applied fields is the structure acquired by the spontaneous emission spectra, and especially the influence of the spontaneous decay rates in setting the strength of the emitted intensity and the width of each of the spectral components. In particular, spectral features that may be unresolved for a certain selection of operating parameters [see, for example, Fig. 6(a)] may become readily observable with a judicious selection of driving field strength. From these results one may be tempted to speculate about the possibility of resolving closely spaced energy levels. Although we have not done detailed calculations to verify this point, it may be interesting to inquire how the predictions of this work may change if one or more of the atomic levels are replaced by pairs of nearly degenerate sublevels. Transient beat effects are known to occur in situations of this type. Here one is interested in the possible existence of recognizable steady-state features that would lead to improved detection of close-spaced atomic lines.

Another unexpected and intriguing phenomenon has to do with the absorption spectrum of a weak probe. We have known for some time that two-level atoms can develop frequency domains in their response to a probe where gain instead of absorption can be observed. This effect, of course, is not the consequence of a state of inversion between the levels of the driven atom and should be interpreted instead as a parametric energy transfer from the pump to the probe, mediated by the atomic susceptibility. In our case a new feature develops: a probe beam can be amplified over practically the entire frequency range of the absorption feature if the dressed atomic levels are driven into a state of inversion. This condition [Eq. (5.52)] can be satisfied rather easily, as shown at the end of Sec. V. The implications of this effect will require additional studies; the most obvious question, of course, concerns the influence of an optical cavity with the ability to resonate at the frequency for which the gain in the atomic response is highest.

One area that was not mentioned in this paper but for which we have some preliminary data has to do with the intensity correlation properties of the fluorescence radiation. This is a subject that has already received considerable recognition in connection with the photon antibunching effect displayed by driven two-level systems and in more recent times within the context of nonclassical fields. In our case we have seen evidence of interesting behaviors with three-level atoms as well. In addition to antibunching, appropriate selections of parameters appear to favor the emergence of anomalously large fluctuations. As we know, narrow-band thermal light can produce excess fluctuations for short delays (the Hanbury-Brown and Twiss effect) which exceed the long delay limit by a factor of 2; in our case we have recorded excess factors of 8 and more in some numerical simulations. Again, these are not transient phenomena, but instead they persist after steady state has been achieved. We plan to analyze this phenomenon in greater detail and to review also the alternative Λ and Ξ configurations. Our findings, if sufficiently interesting, will be the subject of future publications.

Note added in proof. After completion of this manuscript we have been informed by Y. Zhu, D. J. Gauthier, and T. W. Mossberg that they have succeeded in demonstrating the existence of line narrowing with an experiment involving a beam of barium atoms driven by two independent coherent sources in a *V*-type configuration.

ACKNOWLEDGMENTS

We are grateful to Aaron Manka and Heide Doss for sharing with us a preview of their interesting work on the Λ and Ξ systems and to Professor E. Arimondo, Professor J. H. Eberly, Professor T. Mossberg, and Professor C. R. Stroud for informative discussions, suggestions, and comments. We are also grateful to Professor J. M. Centrella for allowing us to use the symbolic logic facilities in her Sun station. One of us (M.O.S.) wishes to acknowledge partial support from the Office of Naval Research.

APPENDIX A: THE DRESSED STATES OF THE QUANTUM MODEL

The construction of the dressed states of the quantum counterpart of the Hamiltonian (2.1) has already been described in earlier publications (see for example, Refs. 15, 19, and 27). Here, for completeness, we outline this derivation. The full quantum model consists of a three-level atom coupled to a pair of electromagnetic modes, with a total Hamiltonian given by

$$H=\sum_{i=2}^{3}\varepsilon_i a_i^\dagger a_i+\hbar\omega_1 b_1^\dagger b_1+\hbar\omega_2 b_2^\dagger b_2 +\hbar(\kappa_1 a_3^\dagger a_1 b_1+\kappa_1^* a_1^\dagger a_3 b_1^\dagger) +\hbar(\kappa_2 a_2^\dagger a_1 b_2+\kappa_2^* a_1^\dagger a_2 b_2^\dagger) , \tag{A1}$$

where ε_i denotes the energy of the ith atomic level (the ground-state energy is chosen equal to zero), $a_i^\dagger$ and a_i are creation and destruction operators for the electrons, $b_i^\dagger$ and b_i the corresponding operators for the field modes, and κ_i $(i=1,2)$ are complex coupling constants. We show that the spectrum of eigenstates of this Hamiltonian can be arranged on a two-dimensional lattice of triplets for every value of the field quantum numbers $n_1>0$ and $n_2>0$. The boundaries of this space, for $n_1>0$ and $n_2=0$ and for $n_1=0$ and $n_2>0$ are comprised of doublets and the ground state (for $n_1=n_2=0$) is a singlet.

It is convenient to write the Hamiltonian in the form

$$H=H_0+H_1 , \tag{A2}$$

where

$$H_0=\hbar\omega_1(a_3^\dagger a_3+b_1^\dagger b_1)+\hbar\omega_2(a_2^\dagger a_2+b_2^\dagger b_2) \tag{A3}$$

and

$$H_1=\hbar\Delta_1 a_3^\dagger a_3+\hbar\Delta_2 a_2^\dagger a_2+\hbar(\kappa_1 a_3^\dagger a_1 b_1+\kappa_1^* a_1^\dagger a_3 b_1^\dagger) +\hbar(\kappa_2 a_2^\dagger a_1 b_2+\kappa_2^* a_1^\dagger a_2 b_2^\dagger) . \tag{A4}$$

The symbols Δ_1 and Δ_2 denote the frequency detunings $\omega_{31}-\omega_1$ and $\omega_{21}-\omega_2$, respectively. Note that

$$[H_0,H_1]=0 . \tag{A5}$$

In the subspace with $n_1>0$ and $n_2>0$ and fixed values of n_1 and n_2 we diagonalize H_1 using the set of eigenstates of H_0

$$|1\rangle|n_1,n_2\rangle,\quad |2\rangle|n_1,n_2-1\rangle,\quad |3\rangle|n_1-1,n_2\rangle ,$$

as a basis. The matrix representation of the interaction Hamiltonian is

$$H_1=\hbar\begin{bmatrix} 0 & \kappa_2^*\sqrt{n_2} & \kappa_1^*\sqrt{n_1} \\ \kappa_2\sqrt{n_2} & \Delta_2 & 0 \\ \kappa_1\sqrt{n_1} & 0 & \Delta_1 \end{bmatrix} \tag{A6}$$

and the eigenvalues are the solutions of the cubic equation

$$\lambda^3-\lambda^2\hbar(\Delta_1+\Delta_2)+\lambda\hbar^2(\Delta_1\Delta_2-|\kappa_1|^2n_1-|\kappa_2|^2n_2) +\hbar^3\Delta_1|\kappa_2|^2n_2+\hbar^3\Delta_2|\kappa_1|^2n_1=0 . \tag{A7}$$

For simplicity we limit our considerations to the resonant case in which Δ_1 and Δ_2 are both equal to zero. If we denote the required eigenstates of H_1 in the n_1,n_2 subspace with $|r,n_1,n_2\rangle$, $|s,n_1,n_2\rangle$, and $|t,n_1,n_2\rangle$, respectively, a simple calculation yields the eigenvalues

$$\lambda_{r,n_1,n_2}=0,\quad \lambda_{s,n_1,n_2}=\hbar G,\quad \lambda_{t,n_1n_2}=-\hbar G , \tag{A8}$$

where

$$G^2=|\kappa_1|^2n_1+|\kappa_2|^2n_2 \tag{A9}$$

and the normalized eigenvectors

$$|r,n_1,n_2\rangle=(\cos\theta)e^{i\varphi_2}|2\rangle|n_1,n_2-1\rangle-(\sin\theta)e^{i\varphi_1}|3\rangle|n_1-1,n_2\rangle , \tag{A10a}$$

$$|s,n_1,n_2\rangle=\frac{1}{\sqrt{2}}[|1\rangle|n_1,n_2\rangle+(\sin\theta)e^{i\varphi_2}|2\rangle|n_1,n_2-1\rangle+(\cos\theta)e^{i\varphi_1}|3\rangle|n_1-1,n_2\rangle] , \tag{A10b}$$

$$|t,n_1,n_2\rangle=\frac{1}{\sqrt{2}}[-|1\rangle|n_1,n_2\rangle+(\sin\theta)e^{i\varphi_2}|2\rangle|n_1,n_2-1\rangle+(\cos\theta)e^{i\varphi_1}|3\rangle|n_1-1,n_2\rangle] , \tag{A10c}$$

where φ_1 and φ_2 are the phases of the complex coupling constants κ_1 and κ_2.

In the subspace with $n_1>0$ and $n_2=0$ we diagonalize H_1 using the basis set

$$|1\rangle|n_1,0\rangle,\quad |3\rangle|n_1-1,0\rangle ,$$

and we find the eigenvalues

$$\lambda_{s,n_1,0}=\hbar|\kappa_1|\sqrt{n_1},\quad \lambda_{t,n_1,0}=\hbar|\kappa_2|\sqrt{n_1} , \tag{A11}$$

and the corresponding eigenvectors

$$|s,n_1,0\rangle=\frac{1}{\sqrt{2}}(|1\rangle|n_1,0\rangle+e^{i\varphi_1}|3\rangle|n_1-1,0\rangle) , \tag{A12a}$$

$$|t,n_1,0\rangle=\frac{1}{\sqrt{2}}(-|1\rangle|n_1,0\rangle+e^{i\varphi_1}|3\rangle|n_1-1,0\rangle) . \tag{A12b}$$

In the subspace with $n_1=0$ and $n_2>0$ we diagonalize H_1 using the basis set

$$|1\rangle|0,n_2\rangle,\quad |2\rangle|0,n_2-1\rangle ,$$

and obtain the eigenvalues

$$\lambda_{s,0,n_2}=\hbar|\kappa_2|\sqrt{n_2},\quad \lambda_{t,0,n_2}=-\hbar|\kappa_2|\sqrt{n_2} , \tag{A13}$$

and the eigenvectors

$$|s,0,n_2\rangle=\frac{1}{\sqrt{2}}(|1\rangle|0,n_2\rangle+e^{i\varphi_2}|2\rangle|0,n_2-1\rangle) , \tag{A14a}$$

$$|t,0,n_2\rangle=\frac{1}{\sqrt{2}}(|1\rangle|0,n_2\rangle+e^{i\varphi_2}|2\rangle|0,n_2-1\rangle . \tag{A14b}$$

Finally, the ground state of H_1 is the singlet

$$|\text{ground}\rangle=|1\rangle|0,0\rangle . \tag{A15}$$

APPENDIX B: DERIVATION OF EQ. (5.19)

The essential step leading to the explicit formulas derived in Sec. V is the replacement of the matrix L that appears in Eq. (5.18) with the block-diagonal matrix L_0 of Eq. (5.19). In order to understand the nature of this approximation consider the explicit form of the equations for $\delta\rho'_{\mu\nu}$. Here we only focus on the first three of the eight independent equations because this will be sufficient for our purposes. We have

$$\frac{d}{dt}\delta\rho'_{st}=-2iG\delta\rho'_{st}+\Gamma_{strs}\delta\rho'_{rs}+\Gamma_{strt}\delta\rho'_{rt}+\Gamma_{stsr}\delta\rho'_{sr}+\Gamma_{stst}\delta\rho'_{st}+\Gamma_{sttr}\delta\rho'_{tr}+\Gamma_{stts}\delta\rho'_{ts}$$
$$+(\Gamma_{stss}-\Gamma_{strr})\delta\rho'_{ss}+(\Gamma_{sttt}-\Gamma_{strr})\delta\rho_{tt}\ , \tag{B1a}$$

$$\frac{d}{dt}\delta\rho'_{sr}=-iG\delta\rho'_{sr}+\Gamma_{srrs}\delta\rho'_{rs}+\Gamma_{srrt}\delta\rho'_{rt}+\Gamma_{srsr}\delta\rho'_{sr}+\Gamma_{srst}\delta\rho'_{st}+\Gamma_{srtr}\delta\rho_{tr}+\Gamma_{srts}\delta\rho'_{ts}$$
$$+(\Gamma_{srss}-\Gamma_{srrr})\delta\rho'_{ss}+(\Gamma_{srtt}-\Gamma_{srrr})\delta\rho'_{tt}\ , \tag{B1b}$$

$$\frac{d}{dt}\delta\rho'_{rt}=-iG\delta\rho'_{rt}+\Gamma_{rtrs}\delta\rho'+\Gamma_{rtrt}\delta\rho'_{rt}+\Gamma_{rtsr}\delta\rho'_{sr}+\Gamma_{rtst}\delta\rho'_{st}+\Gamma_{rttr}\delta\rho'_{tr}+\Gamma_{rtts}\delta\rho'_{ts}$$
$$+(\Gamma_{rtss}-\Gamma_{rtrr})\delta\rho'_{ss}+(\Gamma_{rttt}-\Gamma_{rtrr})\delta\rho'_{tt}\ . \tag{B1c}$$

If we let

$$\delta\rho'_{st}=e^{-2iGt}R_{st},\quad \delta\rho'_{st}=e^{-iGt}R_{sr}\ ,$$
$$\delta\rho'_{rt}=e^{-iGt}R_{rt},\quad \delta\rho'_{ss}=R_{ss},\quad \delta\rho'_{tt}=R_{tt}\ , \tag{B2}$$
$$\delta\rho'_{rs}=e^{iGt}R_{rs},\quad \delta\rho'_{tr}=e^{iGt}R_{tr},\quad \delta\rho'_{ts}=e^{2iGt}R_{ts}\ ,$$

we obtain

$$\frac{dR_{st}}{dt}=\Gamma_{stst}R_{st}+o\ , \tag{B3a}$$

$$\frac{dR_{sr}}{dt}=\Gamma_{srrt}R_{rt}+\Gamma_{srsr}R_{sr}+o\ , \tag{B3b}$$

$$\frac{dR_{rt}}{dt}=\Gamma_{rtrt}R_{rt}+\Gamma_{rtsr}R_{sr}+o \tag{B3c}$$

where o denotes rapidly oscillating terms.

In view of the assumed large value of G, it is reasonable to drop the oscillating contributions so that, in terms of the original variables, we have

$$\frac{d}{dt}\delta\rho'_{st}=(\Gamma_{stst}-2iG)\delta\rho'_{st}\ , \tag{B4a}$$

$$\frac{d}{dt}\delta\rho'_{sr}=(\Gamma_{srsr}-iG)\delta\rho'_{sr}+\Gamma_{srrt}\delta\rho'_{rt}\ , \tag{B4b}$$

$$\frac{d}{dt}\delta\rho'_{rt}=\Gamma_{rtsr}\delta\rho'_{sr}+(\Gamma_{rtrt}-iG)\delta\rho'_{rt}\ . \tag{B4c}$$

Hence, by neglecting the rapidly oscillating components, the new matrix L_0 can be obtained from the original matrix L after ignoring the elements outside the block-diagonal structure composed of the five submatrices as shown schematically below

$$L_0=\begin{bmatrix}(1\times1) & & & & \\ & (2\times2) & & & \\ & & (2\times2) & & \\ & & & (2\times2) & \\ & & & & (1\times1)\end{bmatrix}\ . \tag{B5}$$

*Permanent address: Department of Physics and Atmospheric Science, Drexel University, Philadelphia, PA 19104.

[1]V. Weisskopf and E. Wigner, Z. Phys. **63**, 54 (1930); **65**, 18 (1931).

[2]W. Heitler, *Quantum Theory of Radiation*, 3rd. ed. (Oxford University Press, London, 1954), pp. 36 and 196–203.

[3]M. C. Newstein, Phys. Rev. **167**, 89 (1968).

[4]B. R. Mollow, Phys. Rev. **188**, 1969 (1969); Phys. Rev. A **2**, 76 (1970).

[5]C. R. Stroud, Jr., Phys. Rev. A **3**, 1044 (1971).

[6]G. S. Agarwal, Phys. Rev. A **2**, 2038 (1970); **4**, 1778 (1971); see also *Quantum Statistical Theories of Spontaneous Emission and their Relation to Other Approaches* (Springer, Berlin, 1974), p. 111.

[7]W. Hartig and H. Walther, Appl. Phys. **1**, 171 (1973).

[8]F. Shuda, C. R. Stroud, Jr., and M. Hercher, J. Phys. B **7**, L198 (1974).

[9]F. Y. Wu, R. E. Grove, and S. Ezekiel, Phys. Rev. Lett. **35**, 1426 (1975); R. E. Grove, F. Y. Wu, and S. Ezekiel, Phys. Rev. A **15**, 227 (1975).

[10]H. Walther, in *Proceedings of the Second Spectroscopy Conference, Megève, France, 1974*, edited by S. Haroche, J. C. Pebay-Peyroula, T. W. Hänsch, and S. E. Harris (Springer-Verlag, Berlin, 1975), p. 358.

[11]See, for example, S. Haroche and D. Kleppner, Phys. Today **44**(1), 24 (1989), and references therein.

[12]See, for example, H. Walther, in *Laser Spectroscopy of Atoms and Molecules*, Vol. 2 *of Topics in Applied Physics*, edited by H. Walther (Springer-Verlag, Berlin, 1976), p. 1; see also K. Shimoda, in *ibid.*, p. 198.

[13]E. Arimondo and G. Orriols, Nuovo Cimento Lett. **17**, 333 (1976).

[14]R. M. Whitley, Ph.D. thesis, University of Rochester, 1977; R. M. Whitley and C. R. Stroud, Jr., Phys. Rev. A **14**, 1498 (1976).

[15](a) C. Cohen-Tannoudji and S. Reynaud, J. Phys. B **10**, 345 (1977); (b) **10**, 365 (1977); (c) **10**, 2311 (1977).

[16]H. R. Gray, R. M. Whitley, and C. R. Stroud, Jr., Opt. Lett. **3**, 218 (1978).

[17]G. Orriols, Nuovo Cimento **53B**, 1 (1979).

[18]G. S. Agarwal and S. S. Jha, J. Phys. B **12**, 2655 (1979).

[19]H.-I. Yoo and J. H. Eberly, Phys. Rept. **118**, 239 (1985).

[20]F. Y. Wu, S. Ezekiel, M. Ducloy, and B. R. Mollow, Phys. Rev. Lett. **38**, 1077 (1977).

[21]L. M. Narducci, G.-L. Oppo, and M. O. Scully, Opt. Commun. **75**, 111 (1990).

[22]M. O. Scully, S.-Y. Zhu, and A. Gavrielides, Phys. Rev. Lett. **62**, 2813 (1989); see also A. Imamoglu and S. E. Harris, Opt. Lett. **14**, 1344 (1989); S. E. Harris, Phys. Rev. Lett. **62**, 1033 (1989).

[23]G. S. Agarwal, A. C. Brown, L. M. Narducci, and G. Vetri, Phys. Rev. A **15**, 1613 (1977).

[24]B. R. Mollow, Phys. Rev. A **5**, 2217 (1972).

[25](a) M. Lax, Phys. Rev. **172**, 350 (1968); (b) H. Haken and W. Weidlich, Z. Phys. **205**, 96 (1967); (c) M. Lax, in *Statistical Physics, Phase Transitions and Superfluidity,* edited by M. Chretien, E. P. Gross, and S. Deser (Gordon and Breach, New York, 1968), Vol. 2, p. 269.

[26]H. Haken, in *Laser Theory,* Vol. XXV/2c of *Handbuch der Physik,* edited by S. Flügge (Springer-Verlag, Berlin, 1970), p. 57.

[27]S.-Y. Zhu, J. Mod. Opt. **36**, 499 (1989).